Volume 4
Number 2
February 2024
Pages 107–284

Environmental Science
Atmospheres

rsc.li/esatmospheres

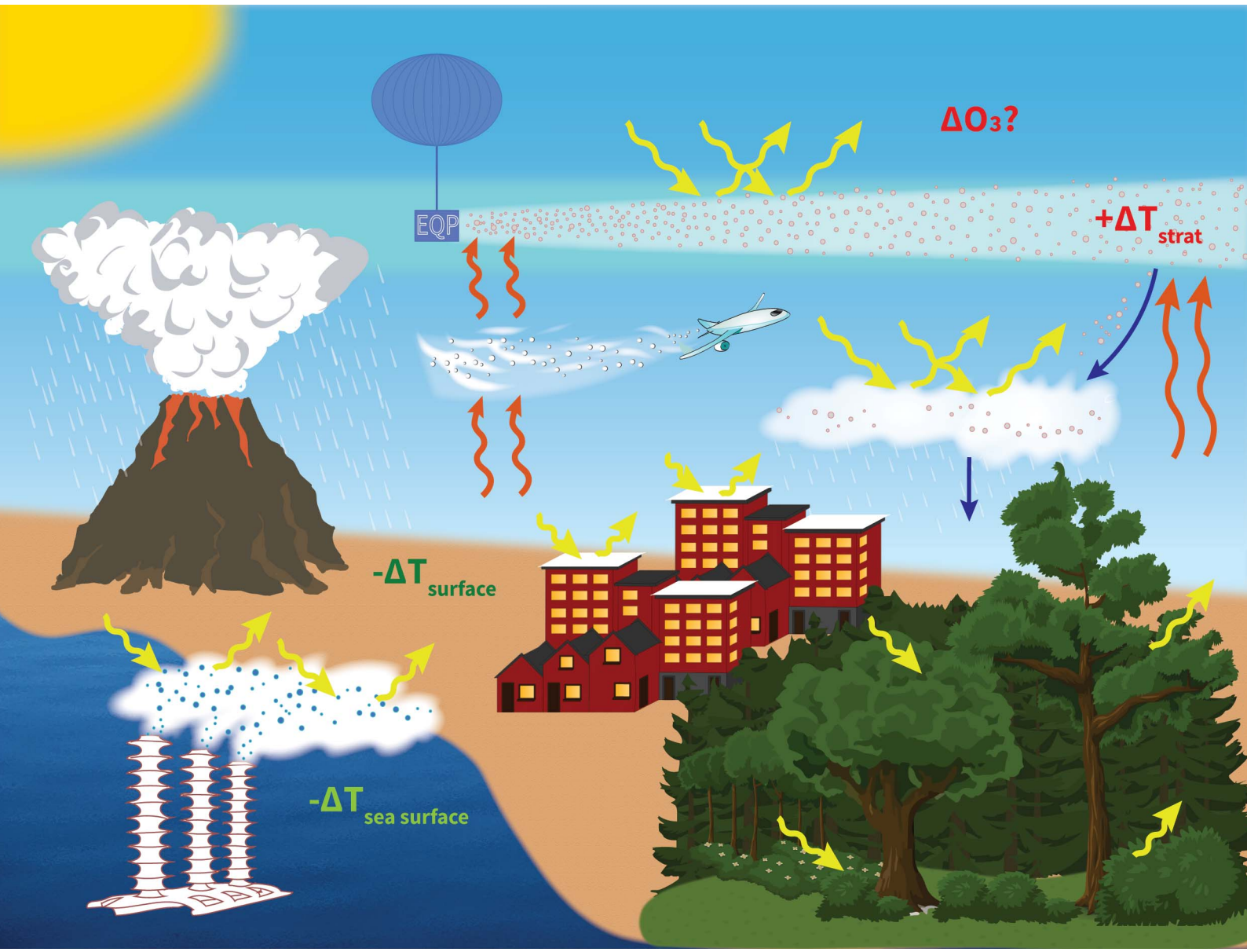

ISSN 2634-3606

ROYAL SOCIETY OF CHEMISTRY

CRITICAL REVIEW
Han N. Huynh and V. Faye McNeill
The potential environmental and climate impacts of stratospheric aerosol injection: a review

Environmental Science: Atmospheres

ROYAL SOCIETY OF CHEMISTRY

CRITICAL REVIEW

View Article Online
View Journal | View Issue

Cite this: *Environ. Sci.: Atmos.*, 2024, **4**, 114

The potential environmental and climate impacts of stratospheric aerosol injection: a review†

Han N. Huynh *[ab] and V. Faye McNeill *[cd]

Given the rise in global mean temperature as a direct consequence of increasing levels of greenhouse gases (GHG) in the atmosphere, a variety of climate engineering approaches, including stratospheric aerosol injection (SAI), have been proposed. Often criticized as a distraction from global efforts towards reducing GHG emissions, SAI aims to increase the Earth's albedo by seeding aerosols in the lower stratosphere. Inspired in part by observations of temporary cooling of the Earth's surface following major volcanic eruptions which introduced significant loadings of sulfate particles into the stratosphere, SAI has been explored extensively in modeling studies. The cooling effect may be accompanied by other significant consequences including stratospheric heating, stratospheric ozone (O_3) depletion, and reduced global mean precipitation. In order to understand the potential environmental and climate impacts of SAI, we review the state of the knowledge regarding these issues, starting from an aerosol science perspective. We summarize aerosol radiative properties and the role they play in defining the optimal chemical and physical aerosol characteristics for SAI, and their implications for lower stratospheric warming. We then review in depth the impacts of stratospheric aerosol heterogeneous chemistry on global O_3 levels. We review SAI modeling studies as well as their uncertainties, in comparison to the observed environmental and climate impacts of volcanically derived sulfate aerosols, including impacts on global temperature, stratospheric warming, and hydrological cycle. We also briefly discuss the current governance and economic considerations of the application of SAI and raise essential questions from both research and social standpoints that should be addressed before SAI is deployed for climate change mitigation.

Received 8th September 2023
Accepted 15th January 2024

DOI: 10.1039/d3ea00134b

rsc.li/esatmospheres

Environmental significance

Climate engineering approaches, including stratospheric aerosol injection (SAI), have been proposed as climate mitigation tools to complement efforts to reduce greenhouse gas emissions or directly remove greenhouse gases from the atmosphere. SAI consists of injecting aerosol particles into the lower stratosphere which will reflect sunlight back to space, resulting in a cooling effect in the troposphere (lower atmosphere). The cooling effect is accompanied by other significant, potentially negative consequences including heating and ozone depletion in the stratosphere (upper atmosphere), and reduced global mean precipitation. We review the state of the knowledge regarding these issues and raise questions from both scientific and social standpoints that should be addressed before SAI is deployed for climate change mitigation.

1 Introduction

Global anthropogenic carbon dioxide (CO_2) emissions have increased steadily since 1750, with a significant rise between 1970 and 2011 that accounts for almost 50% of the cumulative emissions.[1] The rise in global temperature at both land and ocean surfaces, more frequent observations of extreme weather events, such as tropical cyclones[2,3] and heat waves,[4] together with the projected increase in CO_2 and other greenhouse gas (GHG) emissions,[5] have prompted an increase in international commitment to battle global warming. As a result, the 2015 Paris agreement was adopted by almost 200 countries, setting a goal of limiting global warming to less than 1.5 °C by reducing GHG emissions significantly. However, there have been discrepancies in the estimated global carbon budget[1,6–8] and thus, uncertainty in the required trajectory for emission reduction. In addition, the interpretation and implementation of the nationally determined contributions (NDC) or emission pledges from the participating countries have been inconsistent.[9–11] Depending on the level of pledges from participating countries, how much global warming could be reduced varies.[12] Consequently, there is a risk that, unless the

[a]*Cooperative Institute for Research in Environmental Sciences (CIRES), University of Colorado, Boulder, Colorado, USA 80305*

[b]*National Oceanic and Atmospheric Administration (NOAA), Chemical Sciences Laboratory, Boulder, CO, USA 80305. E-mail: han.huynh@noaa.gov*

[c]*Department of Chemical Engineering, Columbia University, New York, New York, USA 10027. E-mail: vfm2103@columbia.edu*

[d]*Department of Earth and Environmental Sciences, Columbia University, New York, New York, USA 10027*

† Electronic supplementary information (ESI) available. See DOI: https://doi.org/10.1039/d3ea00134b

global mitigation efforts are strengthened, total carbon emissions may remain relatively constant by the near-term target of 2030.[13] Therefore, concurrently with the efforts of lowering GHG emissions, many different climate interventions, or 'geoengineering' techniques, have been proposed and researched extensively (Fig. 1).

Radiative forcing geoengineering (RFG) has been considered since at least the 1950s.[14–16] RFG comprises two main categories that focus on increasing either the outgoing terrestrial longwave (LW) radiation escaping from the Earth's surface to space (*i.e.*, Cirrus Cloud Thinning, CCT)[17] or the amount of incoming shortwave (SW) solar radiation reflected back to space (solar radiation management – SRM).[18] SRM techniques include Surface Albedo Geoengineering (SAG), Marine Cloud Brightening (MCB), and Stratospheric Aerosol Injection (SAI).

1.1 Cirrus cloud thinning (CCT)

Cirrus clouds are optically thin clouds made of ice crystals that are located in the upper troposphere. They were observed to have a strong impact on the global top-of-atmosphere (TOA) LW radiative fluxes and, thus, an overall warming effect on the climate.[19] First proposed by Mitchell and Finnegan in 2009,[17] CCT involves seeding cirrus clouds with efficient heterogeneous ice nuclei, such as bismuth tri-iodide, to enable the nucleation and growth of ice crystals, resulting in a quicker sedimentation out of the clouds. The resulting optically thinner cirrus clouds were modelled to reduce the amount of trapped infrared radiation in the atmosphere, leading to a net cloud forcing of about -2 W m^{-2} and a temperature drop of $\sim$1.4 K (ref. 20 and 21) at the Earth's surface. In addition to the net cooling impact, CCT was also predicted to enhance the hydrological cycle, including the strengthening of the Indian monsoon.[22] However, over-seeding cirrus clouds with ice-nucleating particles could result in a net warming effect.[20,23] The climatic responses to cirrus cloud seeding are also uncertain depending on the seed particle size, properties, ice saturation ratio, *etc.*[24–26] For example, CCT was simulated to increase the frequency of extreme precipitation events in the Sahel and Central America regions albeit decrease them in other regions globally.[27]

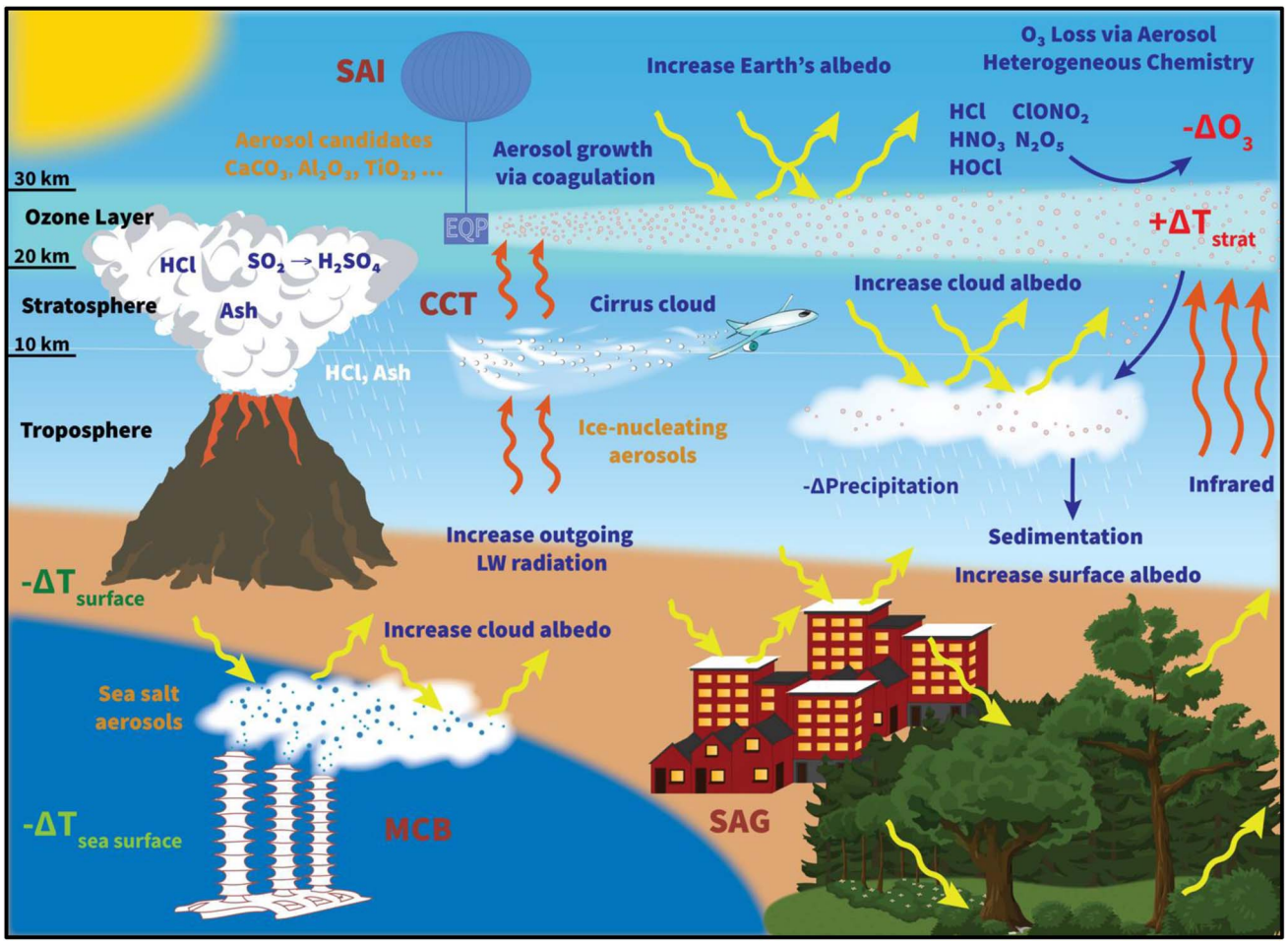

Fig. 1 An illustration of climate geoengineering techniques, including stratospheric aerosol injection (SAI), cirrus cloud thinning (CCT), and marine cloud brightening (MCB), and their proposed delivery systems and potential impacts. Natural stratospheric aerosol release from a volcanic eruption is also shown for context. Surface albedo geoengineering (SAG), which is based on increasing the albedo of various surfaces, is also represented with two examples: installing white roofs on urban buildings and modifying plants and shrubs surface. See the text for details.

1.2 Surface albedo geoengineering (SAG)

Unlike CCT, surface albedo geoengineering (SAG) focuses on increasing the Earth's albedo (*i.e.* the amount of incoming shortwave radiation being reflected back into space). A wide variety of surface albedo modifications have been explored, including increasing the albedo of desert,[28] cropland,[28,29] grassland,[30] and urban environment.[31–33] If plants and shrubs, which cover up to 7.5% of the Earth's surface,[28] were bioengineered to increase their albedo by 25%, a radiative forcing (RF) of about -0.5 W m^{-2} would be achieved.[15,30] At the same time, modifying crops to increase their albedo by 80% (ref. 29) would lead to a RF of -0.35 W m^{-2}, assuming the crops are present year-round over an area as large as 1.4×10^{13} m^2.[34] In addition to modifying vegetation, albedo enhancement to urban regions has the ability to combat the growing problem of urban heat islands (UHI),[35,36] which was calculated to contribute up to 4% of gross global warming.[37] UHI was defined by Oleson and company (2010) as the difference between "the air temperature in the urban canopy layer to the 2 m air temperature from the "rural" surfaces (*i.e.* the vegetated and bare soil surfaces)."[38] By increasing the roof albedo in their simulation, the authors determined that the annual mean heat island in the control simulation decreased from 1.2 °C (in the base case) to 0.8 °C, equivalent with a 33% reduction in UHI. Thus, many cities in the US have started to implement cool roofs.[39] However, there are regional and seasonal limitations to the cooling effectiveness of all of the SAG techniques mentioned here. For example, Oleson *et al.* (2000) found that, in the winter, the use of white roofs to mitigate UHI is less efficient at high latitudes because of the high albedo of deposited snow on the roofs, the reduction in incoming solar radiation, and the concomitant increase in required space heating. As a result, the cooling effect of white roofs may only be local.[37,38] Irvine *et al.* (2011) determined that by changing surface albedo over the global desert area, the annual average surface air temperature decreased by 1.1 °C. Similar to urban and crop geoengineering, the cooling effect was simulated to have regional disparity, where the desert regions such as Sahara were significantly cooler than other continental areas (-10 °C *vs.* -1.1 °C).[28] In general, due to the dependence of all SAG methods on land coverage, the Northern Hemisphere (NH) is more effectively cooled than the Southern Hemisphere (SH). The regional impacts of SAG are discussed in more detail for different climate extreme scenarios in Seneviratne *et al.* (2018).

1.3 Marine cloud brightening (MCB)

Beyond the SAG techniques, other notable SRM options that have been extensively researched are MCB and stratospheric aerosol injection (SAI) (Fig. 1). The proposed concept of MCB[40,41] is to inject sea salt aerosols into the marine boundary layer to increase the cloud droplet number concentrations, and therefore the albedo of the low-lying clouds, due to their enhanced surface area concentrations.[42] The increase in cloud condensation nuclei (CCN) concentrations also results in a reduction in droplet size, and subsequently an increase in the cloud lifetime.[43] As a result, the degree of MCB's cooling effect could, in principle, be controlled by adjusting the spraying rate of the seeding maritime aerosols.[44] Over the ocean, the effects of aerosols on marine clouds have previously been observed in ship tracks or other particle-laden pollution plumes.[45] Computer simulations have yielded favorable results for MCB application. Randall *et al.* (1984) estimated that a 4% increase in marine stratus clouds could offset the global warming impact caused by the doubling of CO_2 level.[46] Similarly, Latham *et al.* (2008) simulated that, under optimal cloud seeding conditions where >25% of the ocean surface is covered, a minimum globally averaged RF of -3.7 W m^{-2} could be achieved.[44] MCB was also modelled to restore precipitation and sea ice values from the impact of increasing GHG concentrations. Specifically, Rasch *et al.* (2009) computed that if ~70% of the ocean surface was seeded monthly over an 80 year period, polar sea ice in the NH would recover to within 2% of 2009 value and that in the SH would increase by 20%. Without cloud seeding, the control case, where CO_2 level was doubled over a 100 year period, yielded about 20% and 36% loss in sea ice area over the NH and SH, respectively.[47] However, there are uncertainties in the albedo response to MCB from the variations in the cloud structure (*e.g.*, closed *vs.* open cell)[48] and in cloud altitude,[49] to name a few. Additionally, similar to the SAG methods, MCB may only have a regional cooling impact, with a focus on the ocean and coastal areas. In addition, the climate impacts of MCB were simulated to be region-dependent, where precipitation was predicted to decrease drastically in the Amazon rain forest.[50] Horowitz *et al.* (2020) determined that by injecting sea salt aerosols throughout the tropics to offset the 4.5 W m^{-2} RF from the Representative Concentration Pathway 4.5 scenario (RCP4.5), tropospheric reactive chlorine and bromine species would increase leading to a 2–4% reduction in surface ozone. Subsequently, OH production would decrease resulting in a 3–6% increase in methane lifetime.[51] The 2020 study findings suggest that MCB may have implications on air quality in coastal regions. Aside from implementation limitations (*e.g.*, creation and dissemination of CCN),[52–54] many environmental and meteorological concerns have been identified that require further study before MCB deployment, such as the potential salt damage to soils and plants,[55] the climate feedback of the increase in land–ocean temperature contrast (*e.g.*, tropical circulation), and the radiative effect of changing CCN in higher-level clouds.[41,44,56,57] Recent studies have investigated the effects of MCB in more comprehensive models as well as implementation methods such as sea salt aerosol sprayers system.[58–60]

1.4 Stratospheric aerosol injection (SAI)

Proposed as a temporary relief to counterbalance the rapid rise in global mean temperature, SAI involves seeding aerosols in the lower stratosphere to harness their reflectivity to offset the positive anthropogenic RF.[61–64] The field of SAI, first proposed by Budyko in 1977,[65] is inspired in part by observations of a global cooling effect[66–68] following major volcanic eruptions.

The eruption of Mt. Pinatubo (15 °N, 121 °E) in June 1991 released large quantities of volcanic materials directly into the stratosphere, including ash and sulfur dioxide gas (SO_2). In the plumes of major explosive volcanic eruptions such as Mt. Pinatubo, SO_2 has the most significant impact on albedo because it

eventually forms sulfate aerosols after getting oxidized by hydroxyl (OH) radicals in the stratosphere. The initial OH oxidation of SO_2 in the Mt. Pinatubo plume was slow due to the depletion of OH radicals by the large cloud of volcanic SO_2.[69] The stratospheric aerosol loading from such major volcanic eruptions greatly perturbs the Earth's radiative balance, leading to a temporary cooling effect in the troposphere as illustrated in Fig. 2.[70] Excessive cooling caused by volcanic eruptions has resulted in volcanic winter, or "year without a summer," with devastating impacts like worldwide food shortage in 1816 following the 1815 eruption of Mount Tambora.[71]

Besides the tropospheric cooling effect, the increase in stratospheric aerosol optical depth (AOD)[72–75] causes warming in the lower stratosphere (~24 km).[66,76,77] For example, after the 1982 eruption of El Chichón (17 °N, 93 °W), tropospheric temperature was cooled by 0.5 °C, while the lower tropical stratosphere was warmed by 3–4 °C.[78,79] Similar observations were made after Mt. Pinatubo's eruption in 1991: after being corrected for 1992 El Niño-Southern Oscillation (ENSO) the tropospheric cooling was ~0.5 °C as shown in Fig. 2, while stratospheric warming was 2.5 °C.[68,80] In the presence of a significant loading of strongly absorbing aerosols like sulfate, the rise in temperature, especially at the tropical tropopause layer (TTL), drives up the amount of water vapor entering the stratosphere.[81,82] Since stratospheric water vapor (SWV) is a GHG, this increase leads to further warming in the stratosphere,[81,82] resulting in changes in the stratospheric–tropospheric tropical circulation[83–85] and accelerating stratospheric ozone depletion.[81,86,87] In particular, stratospheric heating induces major dynamic climate feedbacks such as enhancement in tropical upwelling and extratropical downwelling in the SH, affecting the Brewer–Dobson circulation (BDC) in the stratosphere as well as the global O_3 budget (*e.g.*, the O_3 stratosphere–troposphere exchange (STE) process)[88–93] (more details in Section 3). In the scenario of submarine volcanic eruption like that of Hunga Tonga-Hunga Ha'apai (HTHH) in the South Pacific (20 °S, 175 °W) in 2022, more than 100 Tg of water was injected directly into the stratosphere, contributing up to 10% of global stratospheric water.[94,95] The increased stratospheric water burden enhanced the conversion rate of SO_2 to sulfate, leading to a quicker increase in stratospheric AOD. Despite the initial observed radiative cooling, the presence of large SWV from HTHH eruption was modelled to ultimately lead to a net warming of the climate system.[96,97]

Beyond stratospheric heating, volcanically derived sulfate aerosols also chemically react with gas-phase reservoir species of ozone (O_3) catalytic loss cycles, such as HNO_3, HCl, and N_2O_5, resulting in significant O_3 depletion at mid-latitudes in the stratosphere, which has been observed by TOMS and ground spectrophotometers after the eruptions of both Mt. Pinatubo and El Chichón.[98–101] In both eruptions, O_3 depletion reached about 10% between 16–19 km and 20% between 13–22 km in altitude.[68,79,80] Stratospheric O_3 depletion leads to an increase in UV-B radiation at the Earth's surface in the polar regions,[102] causing adverse effects on human health, marine and terrestrial species such as DNA damage and an increased risk of cancer.[103,104]

The climate impacts of SAI would depend strongly on how, where, and for how long aerosols or their gas-precursor are injected in the atmosphere. While volcanic eruptions are one-time pulsed injections, ideal SAI scenarios generally involve continuous or periodic injection due to the larger particle sizes and hence reduced albedo and shorter lifetime in the atmosphere.[81] The total injected amount of either aerosols (*e.g.*, calcite) or their gas precursor (*e.g.*, SO_2 in the case of sulfate aerosol) will depend upon the climate scenarios (*i.e.*, how much radiative forcing is desired), the extent of their impacts on the atmosphere (*e.g.*, stratospheric ozone chemistry, cirrus clouds, *etc.*),[105–107] and the injection scheme. Ideal engineered deployment scenarios are also different from more complex ones which may be affected by, for example, unexpected environmental disturbances or uncoordinated actors. Nevertheless, as some of the only examples of large aerosol loadings in the lower stratosphere, observations of volcanic eruptions and of their environmental and climate impacts are informative.[108]

Depending on the climate scenario (*i.e.*, the degree of cooling, the continuous or periodic injection rate of aerosol material, the injection location, the termination scheme), SAI could be designed[109] to minimize its negative environmental and public health impacts.[110] For example, Eastham *et al.* (2018) approximated that at a continuous aerosol injection rate of 1 Tg S per year, the increase in UV exposure will lead to an increase in mortality. Yet that would be offset by the gains in improved regional air quality due to reduced surface O_3 exposure.[111] In the study by Madronich *et al.* (2018),[112] about 40 Tg SO_2 per year by 2080 was injected annually at four predetermined locations (15 °S, 15 °N, 30 °S, 30 °N) to keep the global temperatures at 2020

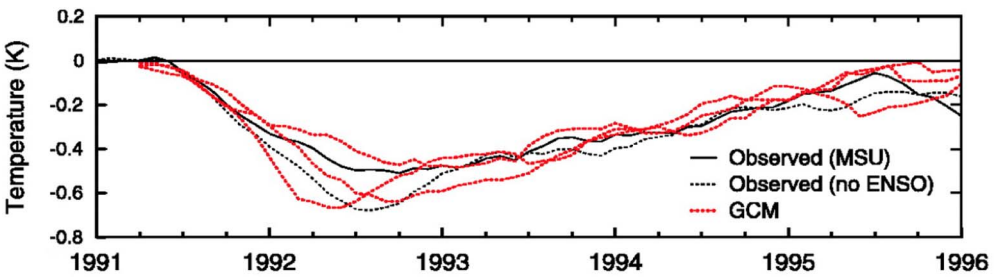

Fig. 2 The observed (black lines) global-mean (90 °N–90 °S) changes in the lower tropospheric temperature compared to the modelled result (dashed red) after Mt. Pinatubo's eruption in June 1991. From Soden *et al.*, *Science*, 2002, **296**, 727–730. Reprinted with permission from AAAS.

levels. UV radiation in this case was modelled to reduce substantially globally and across all seasons. Regardless of their benefits or potential environmental risks, there have long been discussions about how SAI and other SRM studies could weaken the resolve around mitigations efforts to reduce GHGs emission.[113–117] However, recent controlled studies have determined that the potential deployment of SAI or SRM either has no effect on or increases the support of the surveyed public on climate mitigation technologies (*e.g.*, carbon capture).[116,118,119] In addition, some modeling studies suggest that SAI could reduce the global carbon burden and therefore ocean acidification *via* various pathways.[120–122] For example, by inducing sea surface temperature cooling, SAI improves the carbon uptake of the marine environments.[123] However, in the case of a sudden SAI termination, carbon burden has been projected to increase rapidly, causing a worse effect on the environment than the absence of SAI.[120,124–126] As a result, SAI implementation most likely requires a gradual reduction in aerosol injection as the rise in GHG levels slows down in the future. A combination of SAI application and reduction in GHGs emission may yield the best outcome.[127]

To understand the applicability of SAI to offset the rapid rise in global surface temperature, a variety of models and related frameworks has been proposed and extensively studied over the years, many of which are summarized in the 2022 WMO Ozone Assessment report.[110] The overall uncertainties associated with SAI are also discussed in detail in Kravitz and MacMartin (2020).[106] In this review, our goal is to examine in depth various aspects of SAI with a focus on its foundation – aerosols. Specifically, aerosol radiative properties and their significant role in SAI application design are discussed in Section 2. Lower stratospheric heating due to elevated aerosol loadings, and potential ways to mitigate that unintended consequence of SAI, are also examined in Section 2. The negative impacts of aerosol heterogeneous chemistry on the global O_3 budget are covered in detail in Section 3, where we mainly focus on the mechanism behind stratospheric O_3 depletion in Section 3.1. The chemical mechanisms behind changes in tropospheric O_3 due to both aerosol chemistry and the reduction in atmospheric water vapor as a direct result of global cooling[128] are included in Section 3.2. We explore the SAI impact on other aspects of the climate system, such as the hydrological cycle, extreme weather events, and biodiversity in Section 4. Regarding international governance and economic framework for SAI research, implementation and maintenance, we offer a summary of current research and proposals in Section 5. Section 6 includes suggestions and recommendations for future research that is needed to evaluate SAI's applicability for climate mitigation, including uncertainties regarding SAI technology (*e.g.*, seeding aerosols lifetime, termination strategy) and its human health and social impacts.

2 Aerosol radiative properties

The capabilities of atmospheric aerosols to scatter or absorb solar radiation at different wavelengths, collectively referred to as the aerosols' optical properties, have direct effects on the Earth's radiative budget.[68,129] The background stratospheric aerosol layer, located between 15 and 25 km in altitude, consists of aerosols either transported *via* different pathways from the TTL[130] or formed after volcanic eruptions. Together with tropospheric SO_2, carbonyl sulfide (OCS), a chemically inert species, is the main contributor to non-volcanic background sulfate aerosols. OCS and tropospheric SO_2 enter the stratosphere through stratosphere–troposphere exchange (STE),[131,132] where up to 80% of OCS undergoes photodissociation to form SO_2.[131] SO_2, in turn, converts into sulfate particles mainly *via* its reaction with OH radical in the free troposphere and lower stratosphere.[133] Explosive (Plinian) volcanic eruptions perturb the aerosol loading in the stratosphere. Within a month after Mt. Pinatubo's eruption in 1991, the resulting volcanically derived sulfate aerosols dispersed longitudinally covering up to 42% of the Earth's surface[72] and increasing the stratospheric opacity of the tropics between 20 °S and 30 °N latitudes[72,73] by approximately two orders of magnitude as measured by SAGE II[75] (left, Fig. 3). This significantly thicker stratospheric aerosol layer at the tropics increased outgoing SW radiation and lowered the global-mean tropospheric temperature as much as 0.6 °C by the end of 1991 (ref. 68 and 128) (Fig. 2). By the end of 1992, the transient negative forcing produced by Mt. Pinatubo's eruption, about -3 W m^{-2}, exceeded the global climate forcing ($\sim$2 W m^{-2}) that was caused by the rise in GHG from pre-industrial (PI) to 1990 (1850–1990).[68] This observation further proved the remarkable impact stratospheric aerosol could have on cooling the climate, albeit temporarily. Furthermore, even though the AOD decreased by an order of magnitude from the time of the eruption until September 1993 (right, Fig. 3) due to gravitational sedimentation,[68] the remaining loading of sulfate aerosols in the stratosphere was still significant enough to result in a surface cooling effect that persisted till at least 1994 (ref. 128 and 134) as demonstrated in Fig. 2.

Aerosol and chemical species transport from the equator to the poles following volcanic eruptions are driven by stratospheric circulation, Brewer–Dobson circulation (BDC), which also changes seasonally.[92] Based on the timing, location, and magnitude of SAI, the climate response differs.[135] For example, Tilmes *et al.* (2017) determined that if 12 Tg SO_2 per year was injected over a 10 year period at 15 °N at 5 km above the tropopause, the surface temperature would drop about 0.2 °C per Tg S per year. The same SO_2 amount being injected at 1 km above the tropopause would lead to a reduction of 0.12 °C per Tg S per year instead.[136] Visioni and co-authors (2019) further determined that aerosol injection limited to the spring season at either 15 °N or 15 °S resulted in a higher global AOD than that done year-round.[137]

2.1 Aerosol size

Aerosol particle size plays an important role in their radiative effects[138,139] and has been taken into account in SAI models.[86,140–143] Lacis *et al.* (1992) illustrated that if the effective radius of a stratospheric aerosol exceeds $\sim$2 μm, its infrared absorptivity could exceed the albedo effect.[144] In the case of Mt. Pinatubo's eruption, the aerosol effective radius was estimated

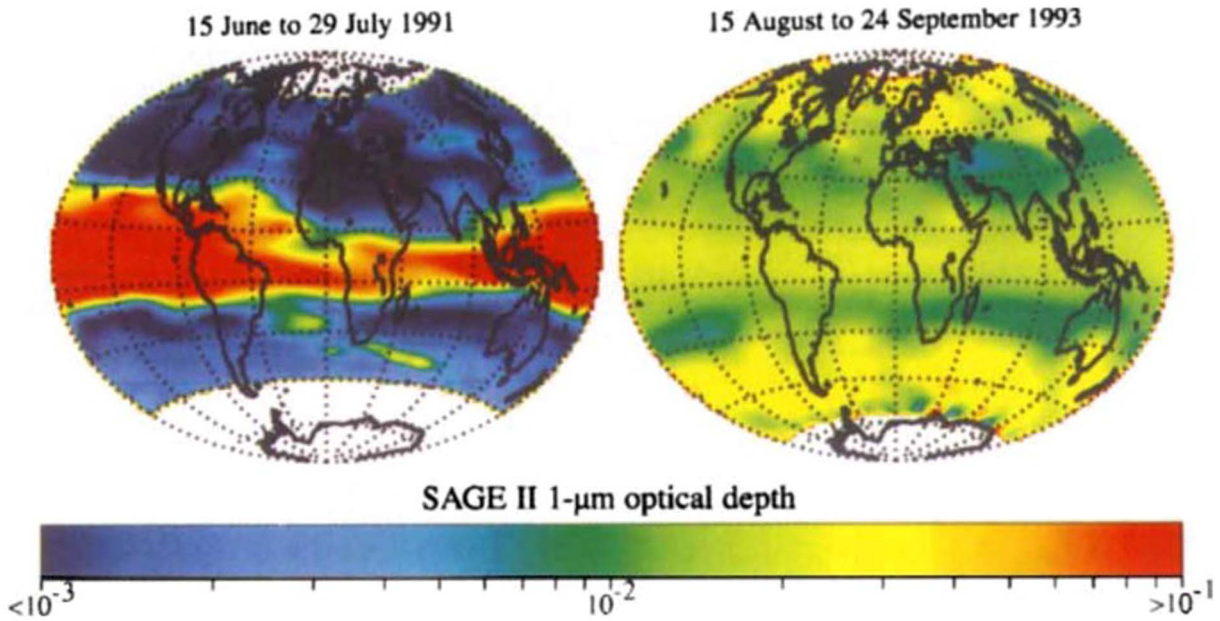

Fig. 3 Stratospheric aerosol optical depth, measured by the stratospheric aerosol and gas experiments-II (SAGE II), was observed to confine in the tropics immediately after Mt. Pinatubo's eruption in June 1991 (left), before the aerosols were dispersed two years later (right). Reprinted with permission of the publisher from McCormick *et al.*, *Nature*, 1995, **373**, 399–404.

to increase from an average of 0.3 μm to roughly 1 μm.[145,146] The observed cooling effect[78] after this eruption is consistent with the aerosol size evaluation by Lacis *et al.* (1992). In addition, aerosol size directly affects its lifetime in the stratosphere[147,148] and hence the duration of its radiative impact.

Aerosols have indirect effects on the Earth's climate by impacting the concentrations and variations of both CCN[149] and ice nuclei.[150,151] This nucleation ability of aerosols is exploited in both CCT and MCB proposals,[17,40] as discussed in Section 1. For SAI application, once aerosols are transported from the stratosphere to the lower troposphere *via* gravitational settling,[148,152] the ensuing aerosol–cloud interactions may have unintended, albeit uncertain, consequences on the hydrological cycle (*e.g.*, reduced precipitation[153–156]) (see Section 4.1 for more discussion of this issue). In addition, similar to CCT and MCB, the increase in the number of available aerosols to act as CCN could also reduce the mean size of the cloud droplets, leading to an enhancement in the cloud albedo.[42,157] A positive change in the cloud albedo effect would prompt more light reflection and thus a cooling effect. Schmidt *et al.* (2012) estimated that, by including a hypothetical global volcanic sulfur flux based on volcanic emission inventories, cloud droplet number concentrations could increase by 10% under 2012 conditions.[158] Similar to the range stated in the 2007 IPCC report,[159] the authors calculated a total cloud albedo forcing range of roughly −0.5 to −1.7 W m^{-2}, including the effects of both anthropogenic (or background) aerosols and volcanic aerosol.

2.2 Aerosol optical properties

How much a change in stratospheric aerosol loading impacts the global radiative forcing depends not only on AOD but also on aerosol composition and its corresponding optical properties. Wavelength-dependent aerosol refractive index, which includes a real index and an imaginary index, accounts for how much light would refract and be absorbed, respectively, by an aerosol particle. An estimate of SW refractive index for various aerosol types were calculated by Dykema and co-authors (2016) and illustrated in Fig. 4. The real refractive index is more frequently available through experimental measurement. The imaginary refractive index, which accounts for the aerosol's absorption capability, may be measured or calculated based on methods used for astronomical applications.[160] For solid aerosol materials, uncertainties in their refractive index values also come from potential defects and impurities in the material. Their refractive index also needs to be corrected for birefringence.

For SAI application, aerosol absorption across both SW and LW has an impact on the level of stratospheric heating. For example, since diamond aerosols have no dipole moment, it has a very low imaginary refractive index (orange line in Fig. 4) compared to $CaCO_3$ (grey line) and therefore absorbs LW radiation minimally. In contrast, sulfate aerosols (yellow line) absorb strongly in the infrared region due to the continuum absorption of their liquid phase. In fact, sulfate has a stronger absorption capability than most of the studied solid materials as shown in Fig. 4. For solid aerosol optical properties, besides their complex refractive index, SAI models also need to account for their fractal aggregates especially upon injection.[161]

2.3 Aerosol types

Sulfate aerosols, the main component of background stratospheric aerosols[162] as well as those produced after volcanic

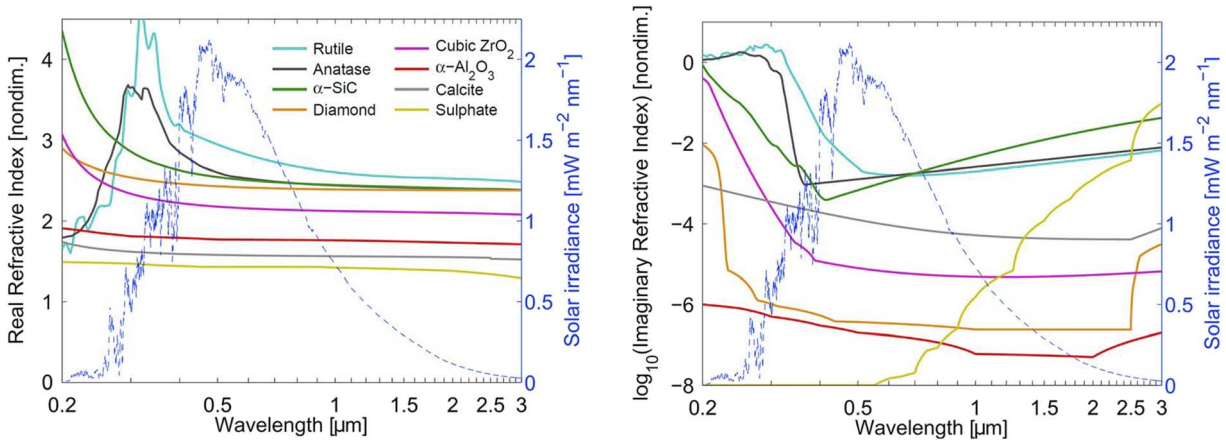

Fig. 4 Shortwave real (left) and imaginary (right) refractive index of different aerosol types based on both available experimental data and estimates from model dielectric functions. Reprinted with permission of the publisher from Dykema *et al.*, *Geophys. Res. Lett.*, 2016, **43**, 7758–7766.

eruptions,[130] have their radiative effects observed[66–68] and modelled[89,163,164] in numerous studies over the decades. Beyond tropospheric cooling effect, aqueous sulfate aerosols produced from volcanic injections were determined to cause localized heating in the lower stratosphere (30–100 hPa)[70] by absorbing solar near infrared radiation and upwelling LW radiation from the surface.[165–167] The extent of stratospheric radiative heating post-volcanic eruptions varies with latitude and altitude.[140,166] It depends strongly on stratospheric aerosol loading or AOD.[70,81,168] The phase of the quasi-biennial oscillation (QBO) at the time of the eruption is also an important factor in the case of tropical injections.[169–171] Fig. 5 illustrates the temperature anomaly in the stratosphere as a result of major volcanic eruptions mostly in the 20th century. For example, ~30 Tg stratospheric aerosol loading of Pinatubo[75] increased the lower tropical stratospheric temperature at 50 hPa by ~4 °C (ref. 70) in 1991. Previously, Labitzke *et al.* (1992) also reported significant stratospheric heating in 1991 at 30 hPa and 20 °N with the biggest spike in September at 2.5 °C, about 3 standard deviations higher than the 26 year monthly mean (1964–1990).[66] As demonstrated in Fig. 5, the largest recorded eruption between 1870 and 2000 was that of Krakatau (1883). Approximately 50 Tg of stratospheric aerosols[172] was loaded resulting in a volcanic AOD of ~0.15 at 550 nm between 30°S and 30°S compared to that of <0.10 from Mt. Pinatubo's eruption.[173] As a result, the stratospheric heating in 1883 was substantially higher than that in 1991 (~5.5 °C *vs.* ~4 °C).[70] Overall, Fig. 5 shows that the observed and modelled temperature response in the lower stratosphere scaled with the measured volcanic AOD.

With the current knowledge of aerosols' direct and indirect climate forcing effects, besides sulfate many different types of aerosols have been proposed[18,141] and explored in the context of SAI, including but not limited to black carbon (BC),[86,87,140] titanium dioxide (TiO_2),[87,140,161] alumina (Al_2O_3),[142] and limestone[140,143,161,174] as summarized in Table 1. Sulfate is the most well-studied stratospheric aerosol due to its enhancement after volcanic eruptions. As a result, many SAI scenarios have been modelled using sulfate to offset different GHG trajectories set out by the IPCC.

By varying SAI parameters (*e.g.*, aerosol loading, aerosol injection location, frequency, duration), the models yielded scenarios, for example, with minimal stratospheric warming.[81] A commonly used IPCC climate scenario, RCP6.0, is a scenario where a RF of 6.0 W m^{-2} may be caused by GHGs in 2150.[180] Xia *et al.* (2017) modelled a sulfate scenario, G4SSA, based on Tilmes *et al.* (2015)[181] for the period between 2020 and 2069 that decreased the TOA solar flux by 2.5 W m^{-2} compared to RCP6.0 as seen in Table 1. For G4SSA a constant sulfate aerosol surface area distribution at 60 mb was added at the beginning of the

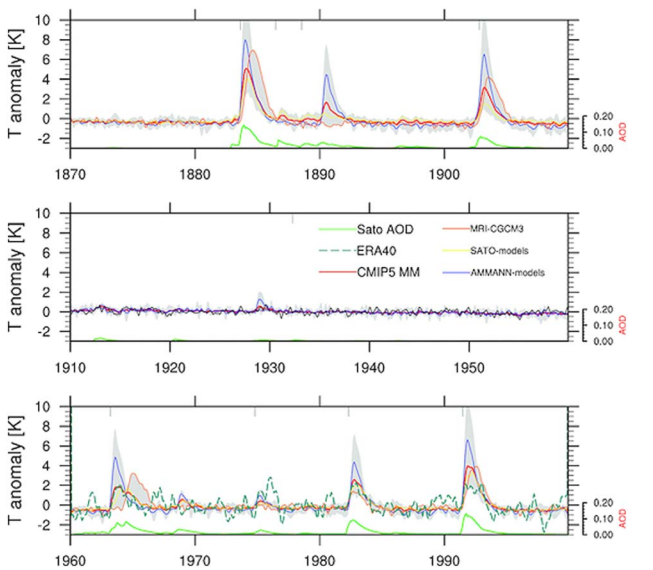

Fig. 5 Stratospheric warming at 50 hPa between 30 °S and 30 °N in the lower stratospheric region after nine major volcanic eruptions in the period between 1870 and 2000 from both historical observations and modeling simulations. Reprinted with permission of the publisher from Driscoll *et al.*, *J. Geophys. Res. Atmos.*, 2012, **117**, 17105.

Table 1 Overview of the modelled anomalies of global mean surface temperature, stratospheric temperature, global ozone column, and global averaged precipitation relative to the base case scenario as a result of SAI implementation in the literature. More details of all listed studies are summarized in Table S1 in the ESI

Base case scenario	Model	SRM scenario	SRM period	Aerosol studied	Particle radius[a] (μm)	Aerosol loading (Tg per year)	Δ Surface temp (K)	Δ Strat. temp[b] (K)	Δ Global ozone column[c] (%)	Δ Precip. (mm per day)	Radiative forcing[d] (W m^{-2})	Year	Ref.
REF2	WACCM3	Geo-eng.	2020–2050	Sulfate	0.43	2	−0.5	1.2	−10[e]	<0.1	—	2009	175
GEO0	AER-2D SOCOLv2.0	GEO1	20 years	Sulfate	0.1	1	—	0.1	−2.3	—	−0.37 ± 0.42*	2009	81
GEO0	AER-2D SOCOLv2.0	GEO2	20 years	Sulfate	0.2	2	—	0.4	−3.2	—	−0.78 ± 0.38*	2009	81
GEO0	AER-2D SOCOLv2.0	GEO5	20 years	Sulfate	0.5	5	—	1.3	−4.5	—	−1.06 ± 0.31*	2009	81
GEO0	AER-2D SOCOLv2.0	GEO10	20 years	Sulfate	0.6	10	—	2.8	−5.3	—	−1.68 ± 0.42*	2009	81
GEO0	AER-2D SOCOLv2.0	GEO5p12	20 years	Sulfate	0.1	5	—	1.3	−4.6	—	−1.29 ± 0.35*	2009	81
GEO0	AER-2D SOCOLv2.0	GEO5p2	20 years	Sulfate	0.3	5	—	1.3	−4.9	—	−1.64 ± 0.23*	2009	81
2000	GISS ModelE2	Def	2000–2010	BC	0.08	1	−0.38	13	0	—	−0.20	2012	86
2000	GISS ModelE2	HA	2000–2010	BC	0.08	1	−4.92	45	−27	—	−0.95	2012	86
2000	GISS ModelE2	SmR	2000–2010	BC	0.03	1	−9.45	60	−47	—	−1.97	2012	86
2000	GISS ModelE2	LgR	2000–2010	BC	0.15	1	−0.06	3	0	—	−0.09	2012	86
2000	GISS ModelE2	HALgR	2000–2010	BC	0.15	1	−2.13	25	−13	—	−0.50	2012	86
1991–1995	ECHAM5-HAM	GE	1991–1995	Sulfate	—	5	−4.9	2	—	—	−0.37	2012	164
1901–2000	IGCM	4CO_2 + sulfate	2000–2080	Sulfate	0.1	—	−0.28	—	—	−0.25	—	2014	85
RCP4.5	ULAQ-CCM	G3	2020–2070	Sulfate	—	SAI	—	0.20	−2.8 DU	—	−1.42†	2014	102
RCP4.5	GISS-E2-R	G3	2020–2070	Sulfate	—	SAI	—	−0.03	−2.1 DU	—	−0.21†	2014	102
RCP4.5	ULAQ-CCM	G4	2020–2070	Sulfate	0.61	5	—	0.40	−1.1 DU	—	−1.52†	2014	102
RCP4.5	GISS-E2-R	G4	2020–2070	Sulfate	0.35	5	—	−0.45	−9.7 DU	—	−1.64†	2014	102
RCP4.5	MIROC-ESM-CHEM	G4	2020–2070	Sulfate	0.24	5	—	0.16	−1.1 DU	—	−0.76†	2014	102
RCP4.5	GEOSCCM	G4	2020–2070	Sulfate	0.60	5	—	0.58	−2.1 DU	—	−1.22†	2014	102
—	AER 2-D	—	10 years	Al_2O_3	0.08	4*	—	—	−10	—	−0.1	2015	142
—	AER 2-D	—	10 years	Al_2O_3	0.16	4	—	—	−6	—	−0.7	2015	142
—	AER 2-D	—	10 years	Al_2O_3	0.24	4	—	—	−3	—	−1.1	2015	142
—	AER 2-D	—	10 years	Diamond	0.16	4	—	—	−6	—	−1.8	2015	142
RCP8.5	HadGEM2-CCS	GeoSulf	2020–2100	Sulfate	0.376	14	0	7	—	−0.1	—	2016	87
RCP8.5	HadGEM2-CCS	GeoBC	2020–2100	BC	0.0118	0.81	1	76	—	−0.27	—	2016	87
RCP8.5	HadGEM2-CCS	GeoTiO_2	2020–2100	TiO_2	0.045	5.8	0.5	+22	—	−0.15	—	2016	87
RCP6.0	RRTM	Rutile	2040+	TiO_2 (rutile)	0.130	1.3	—	1.9	—	—	−1	2016	161
RCP6.0	RRTM	Anatase	2040+		0.145	1.1	—	0.7	—	—	−1	2016	161

Table 1 (*Contd.*)

Base case scenario	Model	SRM scenario	SRM period	Aerosol studied	Particle radius[a] (μm)	Aerosol loading (Tg per year)	Δ Surface temp (K)	Δ Strat. temp[b] (K)	Δ Global ozone column[c] (%)	Δ Precip. (mm per day)	Radiative forcing[d] (W m^{-2})	Year	Ref.
				TiO_2 (anatase)									
RCP6.0	RRTM	α-SiC	2040+	α-SiC	0.150	0.9	—	0.48	—	—	−1	2016	161
RCP6.0	RRTM	Diamond	2040+	Diamond	0.150	1.0	—	0.05	—	—	−1	2016	161
RCP6.0	RRTM	α-ZrO_2	2040+	α-ZrO_2	0.170	2.1	—	0.09	—	—	−1	2016	161
RCP6.0	RRTM	α-Al_2O_3	2040+	α-Al_2O_3	0.215	2.6	—	0.18	—	—	−1	2016	161
RCP6.0	RRTM	$CaCO_3$	2040+	$CaCO_3$	0.275	2.9	—	0.15	—	—	−1	2016	161
RCP6.0	RRTM	Sulfate	2040+	Sulfate	0.300	3.0	—	1.3	—	—	−1	2016	161
RCP6.0	AER 2-D	Calcite	2040+	$CaCO_3$	0.275	5.6	—	0.2	6.4	—	−2	2016	143
RCP4.5	HadGEM2-ES	G4	2020–2069	Sulfate	0.55	5	−1	—	—	−0.1	—	2017	176
RCP4.5	HadGEM2-ES	G4NH	2020–2069	Sulfate	0.55	5	−1	—	—	−0.7	—	2017	176
RCP4.5	HadGEM2-ES	G4SH	2020–2069	Sulfate	0.55	5	−1	—	—	0.4	—	2017	176
RCP6.0	CESM CAM4-chem	G4SSA	2020–2069	Sulfate	—	8	−0.9	3	−3	−0.07	−2.5	2017	89
RCPP8.5	CESM1 (WACCM)	Low-altitude	2042–2049	Sulfate	0.42	32	−2	15	−28 to 8[f]	−0.4	−4	2018	135
RCPP8.5	CESM1 (WACCM)	High-altitude	2042–2049	Sulfate	0.48	24	−2	10	−40 to 8[g]	−0.6	−4	2018	135
RCP4.5	MPI ESM	G3	2050–2069	Sulfate	—	SAI	−0.88	—	—	0.26	—	2018	177
RCP6.0	AER 2-D	Calcite	2040+	$CaCO_3$	—	5.6	—	—	−5 to 25[h]	—	−2	2020	178
SSP5-8.5	CESM2 (WACCM)	G6sulfur	2020–2100	Sulfate	—	21	−3	7	4 DU[i]	—	−0.2	2022	107
SSP5-8.5	CNRM-ESM2-1	G6sulfur	2020–2100	Sulfate	—	—	−2	5	2 DU	—	−0.2	2022	107 and 179
SSP5-8.5	ISPL-CM6A-LR	G6sulfur	2020–2100	Sulfate	—	40	−3.5	13.5	—	—	−0.26	2022	107 and 179
SSP5-8.5	MPI-ESM1.2-LR	G6sulfur	2020–2100	Sulfate	—	36	−2	11	—	—	−0.25	2022	107 and 179
SSP5-8.5	MPI-ESM1.2-HR	G6sulfur	2020–2100	Sulfate	—	36	−2	11	—	—	−0.25	2022	107 and 179
SSP5-8.5	UKESM1-0-LL	G6sulfur	2020–2100	Sulfate	—	21	−2.5	5	−2 DU	—	−0.3	2022	107 and 179

[a] Particle radius is denoted as either effective, mode, or median radius depending on studies. [b] Around ∼50 mb in the tropics (30 °N–30 °S). [c] Global O_3 column change is given in % unless specified otherwise (*e.g.*, DU). [d] The listed global annual mean net SW RF is calculated at the TOA. If the values are followed by '*' or '†' then the RF is at the surface including cloud adjustments or at the tropopause. (127) net SW only. [e] Maximum ozone loss at high latitudes in the SH. [f] Largest reduction (28%) was observed in the South Pole during ozone hole season, while the 8% increase was simulated for Jan between 30 °N and 60 °N. [g] Largest reduction (40%) was observed in the South Pole during ozone hole season, while the 8% increase was simulated for Jan between 30 °N and 60 °N. [h] O_3 impacts were estimated using gas uptake coefficients that were calculated dependently and independently from the aerosol layer thickness to yield the lower and upper limits, respectively, for O_3 column change. [i] Annual changes in total column ozone (TCO) in the tropics. Impacts in other regions and specific seasons are detailed in the cited reference.

simulation and maintained over the 50 year period. This abrupt change in aerosol loading reflects the Geoengineering Model Intercomparison Project (GeoMIP) G4 scenario as proposed by Kravitz *et al.* (2011).[182] Similar to previous observations, the 2017 study also reported an increase in the lower tropical stratospheric temperature (∼3 K) at 30–50 mb. Besides investigating the effect of sulfate aerosols on stratospheric temperature, Dykema *et al.* (2016) also studied a variety of alternative aerosols to improve aerosol radiative properties for SRM application. Sulfate aerosols have one of the strongest infrared absorptions among the studied materials, leading to an increase of ∼1.3 K in stratospheric temperature.[161] Note that

this heating rate is lower than those observed in the Pinatubo eruption and in Xia *et al.* (2017) due to a smaller induced RF (-1 W m^{-2}) compared to -3 W m^{-2} (ref. 68) and -2.5 W m^{-2},[89] respectively. The model indicated that, among the studied materials, diamond has the smallest stratospheric heating at ~0.05 K due to its minimal absorption of LW and SW radiation. Even though diamond only requires a third of total mass of 70 wt% sulfate to achieve a RF of -1 W m^{-2},[161] the delivered cost per unit weight of diamond is estimated to be about two orders of magnitude higher.[183] Due to their high refractive index, Al_2O_3 and calcite ($CaCO_3$), ubiquitous mineral oxides, were also simulated to have a low rate of stratospheric heating (<0.2 K), which have spurred additional studies to test their applicability.[142,143,178,184] Another mineral SAI candidate, TiO_2, has previously been proposed due to its high refractive index (*i.e.* an efficient light scatterer) compared to sulfate (2.5 *vs.* 1.55 at 0.55 μm),[141] requiring 40% less stratospheric aerosol burden for the same cooling. Nevertheless, despite its strong scattering ability, TiO_2 was modelled to heat the lower stratosphere with a rate five times larger than sulfate[87,161] due to its efficient absorption of solar UV radiation.

In addition to mineral oxide aerosols, BC, predominantly emitted from fossil fuels transportation or biomass burning, was also previously suggested, since only less than 2% of the mass of sulfur would be required to achieve the same cooling as sulfate.[18] BC is often considered the strongest absorber among all atmospheric aerosols, with an estimated total climate forcing of +1.1 W m^{-2}, only second after CO_2.[185] By reducing the amount of incoming solar radiation reaching the surface, BC is capable of cooling the global mean temperature. However, due to its dominant ability to absorb SW radiation, BC's heating pattern varied latitudinally with solar radiation. A significant heating of the stratosphere, upward of +70 °C, was simulated in a scenario where enough BC was injected to maintain the global-mean temperature throughout the 2020–2100 period relative to RCP8.5.[87] BC injection may also result in stratospheric O_3 loss[86] further making BC an undesirable material for stratosphere seeding.

SAI aerosols could cause public health issues once they sediment out of the atmosphere. However, Eastham *et al.* (2018) estimated that aerosol sedimentation contributed less to SAI-driven annual mortality rate than other SAI impacts, such as reduction in precipitation and global mean temperature.[111] The presence of stratospheric aerosol layer increases diffuse radiation that potentially leads to sky whitening[186] and enhanced canopy photosynthesis[187] among other effects. Thus, estimating the LW RF caused by SWV increase, as well as the SW diffusive flux, are important benchmarks for evaluating the efficacy of different aerosols as potential SAI candidates. Dykema *et al.* (2016) estimated that rutile and sulfate had the strongest LW RF at 0.24 and 0.18 W m^{-2}, respectively, due to only SWV, leading to a reduction in their SAI efficacy by ~20%.[161] Rutile and sulfate also have the largest LW RF due to only aerosol. Expectedly, the SAI application of these two aerosol materials causes the most stratospheric heating at 1.9 K and 1.3 K, respectively (Table 1). On the other hand, materials that have the least impact on stratospheric temperature (diamond, Al_2O_3, and $CaCO_3$) were calculated to have the lowest LW RF from SWV (<0.3 W m^{-2}). Considering all the aerosols' radiative effects, as well as economics, $CaCO_3$ and Al_2O_3 were suggested to be the most promising SAI candidates among all the studied materials in this 2016 study. Overall, our current understanding of SAI points to the inevitable heating of the stratosphere despite the variations in aerosol size, composition or change in RF as summarized in Table 1.

3 Aerosol heterogeneous chemistry ozone impacts

In this section we discuss in detail the impacts of SAI on stratospheric and tropospheric ozone levels.

3.1 Stratospheric ozone

Surface chemistry taking place on the surfaces of aerosol particles in the stratosphere plays a role in stratospheric ozone depletion. Here we discuss observations of stratospheric ozone and related chemistry following volcanic eruptions, then we review relevant experimental and modelling studies of stratospheric aerosol chemistry.

3.1.1 Observations following volcanic eruptions. In general heterogeneous chemistry of aerosols could directly and indirectly affect stratospheric O_3. The direct effect results from reactions of chlorine reservoir molecules HCl, HOCl, and $ClONO_2$, on polar stratospheric cloud (PSC) particles (R1)–(R3),[188–192] to convert Cl into more photolabile forms, ultimately forming more chlorine radicals for ClO_x cycles to destroy stratospheric O_3.

$$ClONO_2 + HCl(s) \rightarrow Cl_2 + HNO_3(s) \quad (R1)$$

$$ClONO_2 + H_2O(s) \rightarrow HNO_3(s) + HOCl \quad (R2)$$

$$HOCl + HCl(s) \rightarrow Cl_2 + H_2O \quad (R3)$$

The indirect effect comes from partitioning of reactive nitrogen species (NO_x), specifically the reactive uptake of N_2O_5, by background or volcanic aerosols (R4) to sequester NO_x and therefore slow down NO_x cycle.[188,193,194]

$$N_2O_5 + H_2O(s) \rightarrow 2HNO_3(s) \quad (R4)$$

By trapping HNO_3, a reactive nitrogen reservoir species (NO_y), these aerosol reactions also reduce the amount of NO_x available to convert photolytically active chlorine back to its reservoir species ($ClONO_2$). The reduction of NO_x species coupled with the increase in Cl radicals in the presence of stratospheric aerosols make reactive chlorine species more effective at depleting the O_3 layer than reactive nitrogen species.

The main source of stratospheric chlorine has been anthropogenic chlorofluorocarbons (CFCs), with a minor contribution from volcanic eruptions.[195] The concentrations of CFCs have decreased since the implementation of the Montreal Protocol leading to a reduction in stratospheric ozone loss.[196] However, a recent study by Western *et al.* (2023) reported that

the emissions of five CFCs species (CFC-112a, CFC-113a, CFC-114a, CFC-115, CFC-13) have increased by a factor of 3 between 2010 and 2020 albeit with minimal impact on ozone hole recovery for the time being.[197] In addition to chlorine reservoir, surface emission of N_2O, a greenhouse gas and a primary source of stratospheric NO_x, has accelerated over the last two decades, 43% of which was driven by anthropogenic sources.[110,198,199] With the continuous growth of N_2O budget in the atmosphere, NO_x cycle may impact stratospheric ozone loss more dominantly in the next few decades.

Observations following Mt. Pinatubo's 1991 eruption determined that volcanic HCl did not add significantly to the stratospheric chlorine burden.[200,201] Tabazadeh and Turco *et al.* (1993) also showed in a modeling study that injected HCl was quickly removed in condensed supercooled water droplets.[202] However, recent studies[203–206] have suggested that explosive volcanic eruptions were capable of injecting significant quantities of halogens into the lower stratosphere (*e.g.*, HCl and HF from Hekla's 2000 eruption in Iceland[207,208]). Based on previous volcanic halogen observations, Brenna *et al.* (2019) modelled that an injection of ~3 Mt. chlorine and 9.5 Kt. bromine at 14 °N and 30 hPa would lead to a 20% reduction in global mean ozone column within the first 18 months of a 12 year period.[206] Numerous studies in the 1990s[79,209,210] determined that heterogeneous chemical reactions on the surfaces of aerosols, including both background and volcanically-derived sulfate aerosols, contributed more than 50% of the total O_3 loss averaged globally between 69 °S and 69 °N.[204] The importance of heterogeneous reactions on aerosols was first realized from the observations of polar O_3 depletion on PSCs in both the Arctic and Antarctic lower stratosphere.[188,211] In the presence of significant stratospheric aerosol loading following major eruptions, further reductions of the O_3 column are expected.[212,213] For example, after the eruption of Mt. Pinatubo, there was a significant loss of global O_3 well into 1993 with the global O_3 column mean dropping approximately 6% (~18 Dobson Unit (DU)) by April of that year.[68] The bulk of the O_3 column loss was observed in the tropics below 28 km (ref. 214 and 215) and was as large as 20% near 24–25 km.[67,216] Aside from Mt. Pinatubo, Cerro Hudson at 46 °S also erupted in August 1991, leading to an almost 50% O_3 loss between 11 and 13 km over 30 days.[217] The downward trend of O_3 mixing ratio was driven largely by the significant increase in the available stratospheric aerosol surface area for heterogeneous reactions. The Pinatubo eruption caused the average mid-latitude stratospheric aerosol surface area to jump by a factor of 20 by 1992, from about 1.0 $\mu m^2\ cm^{-3}$ to 20 $\mu m^2\ cm^{-3}$,[193] as illustrated in Fig. 6. The peak aerosol surface area was as high as 35 $\mu m^2\ cm^{-3}$ by the end of 1991.[218] As a result, the ratio of ClO/Cl_y increased by a factor of 3 (Fig. 6), consistent with the aforementioned (R1)–(R3). On the other hand, the NO_x/NO_y ratio was reduced, as expected due to the heterogeneous hydrolysis of N_2O_5 on stratospheric aerosol surfaces (R4) as well as the trapping of HNO_3 *via* (R1) and (R2).[219] This column reduction in NO_x, in particular NO_2, reached as high as 40% at northern mid-latitudes by October 1991.[220] By April 1992, a similar decrease in NO_2 column was also observed in southern mid-latitudes[221] as measured in SAGE II. Similarly, El Chichón's major eruption in 1982 also led to a ~50% drop in NO_2 column and most likely contributed to the substantial loss of stratospheric O_3 between 1982 and 1983.[79,222] As NO_2 was reduced substantially, HNO_3 was observed to increase up to 50% (ref. 223) and 30%,[224] respectively, between 1991 and early 1993 at both northern and southern mid-latitudes.

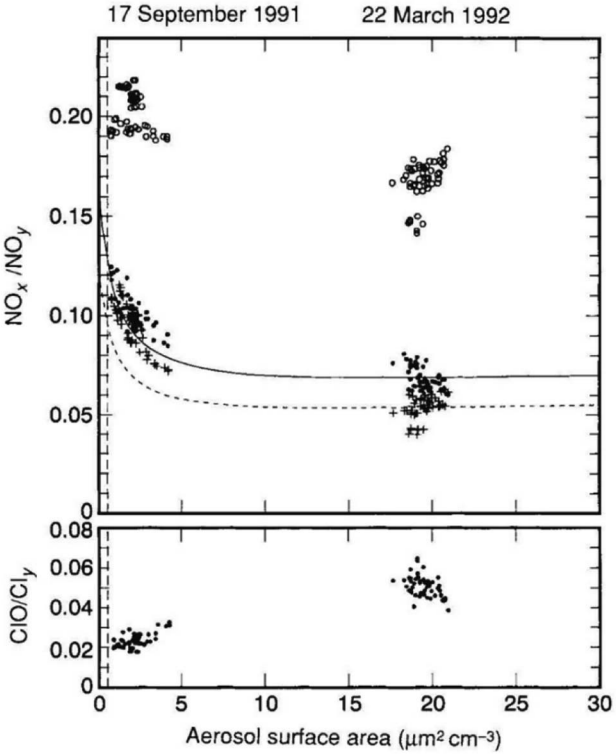

Fig. 6 Measurements of ratios of NO_x/NO_y and ClO/Cl_y (open circles) *versus* the stratospheric aerosol surface area (solid circles) from the NASA Airborne Arctic Stratospheric Expedition II (AASE II) following Mt. Pinatubo's eruption in June 1991. Simulations of aerosol heterogeneous chemistry *via* (R4) are also represented with crosses. Reprinted with permission of the publisher from Fahey *et al.*, *Nature*, 1993, **363**, 509–514.

Despite the general reduction in NO_2 column in both hemispheres after Mt. Pinatubo's eruption, there was a spatial and temporal disparity in the global O_3 loss as measured by TOMS (Fig. 7). In particular, the stratospheric O_3 depletion was mostly concentrated in the NH while there was an observed increase in the O_3 column up to ~10% at the southern middle to high latitudes till the end of 1992.[225–227] Aquila *et al.* (2013) determined that the positive O_3 anomaly in the SH was induced by the enhanced extratropical downwelling, a direct result of stratospheric heating,[90–92] coupled with the downward direction of the BDC at the time of the eruption. This increase in the southern O_3 concentration counteracted the O_3 depletion due to sulfate aerosol heterogeneous chemistry resulting in an overall increase in the O_3 column mean in the SH.[93] The discrepancy between the observed spatial distribution of NO_2 and O_3 columns was most likely because of the shorter timescale of NO_x chemical perturbation compared to that of O_3 depletion.

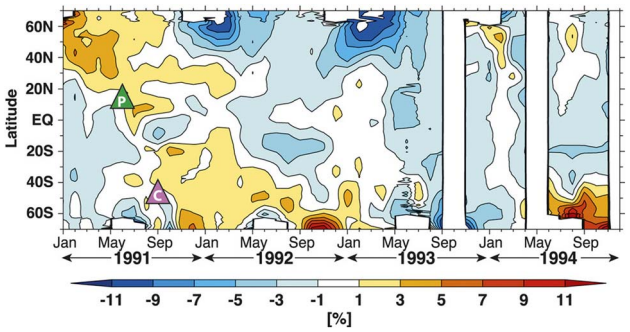

Fig. 7 Zonal mean ozone column change (%) compared to the 1979–1990 baseline from TOMS observation. The green and purple triangles marked the locations of the volcanic eruptions of Mt. Pinatubo (June 1991) and Cerro Hudson (August 1991), respectively. © American Meteorological Society. Used with permission from V. Aquila, L. D. Oman, R. Stolarski, A. R. Douglass and P. A. Newman, *Journal of the Atmospheric Sciences*, 2013, **70**, 894–900.

3.1.2 Experimental studies of aerosol heterogeneous chemistry. SAI aerosol alternatives to sulfate have been studied experimentally in order to better understand their chemical impact on stratospheric O_3. Table 2 summarizes experiments performed on particulate samples of different materials with high potential as SAI candidates. Solid aerosols with high refractive indices are of particular interest, as mentioned in Section 2.

As a common catalysis material and one of the main components of space shuttle solid-fueled rocket motors exhaust,[228] Al_2O_3 heterogeneous chemistry has been studied in the past for its potential stratospheric impact. There is also abundant industrial experience in producing Al_2O_3 nanoparticles[229,230] that would provide great groundwork if Al_2O_3 aerosols were to be used for SAI deployment. However, besides the potential of Al_2O_3's absorption of outgoing terrestrial LW radiation and thus warming the stratosphere,[231] Al_2O_3 was predicted to cause substantial damage to stratospheric O_3 (ref. 232–234) upon release in the atmosphere. Specifically, Molina *et al.* (1997) determined experimentally that (R1) occurred more efficiently on Al_2O_3 particles with an uptake coefficient (γ) of 0.02 than on background sulfate aerosols ($\gamma < 0.0001$) under similar conditions.[235] This would most likely increase chlorine activation that leads to additional stratospheric O_3 depletion.

Besides Al_2O_3 aerosols, other components of mineral dust particles,[236,237] including TiO_2, have also been investigated in terms of their heterogeneous chemistry impact on stratospheric O_3 as listed in Table 2. Since TiO_2 is a well-known efficient photocatalyst that could, for example, convert NO_x species to HNO_3, its heterogeneous reaction with NO_2 has been studied extensively to remove NO_x from the troposphere.[238–241] However, very little data exist for TiO_2 aerosol chemistry with relevant stratospheric gases. Tang *et al.* (2014) reported the first experimental measurement of the heterogeneous reaction of airborne TiO_2 particles with N_2O_5 gas, an important NO_x reservoir species, at ambient conditions over a range of relevant relative humidities (RH) for the lower stratosphere (RH < 40%).[242]

$CaCO_3$, one of the most reactive constituents of mineral dust,[237] was also proposed and studied as a SAI alternative to sulfate aerosols.[140,142,143,161] Yet there is a lack of reliable kinetics data for $CaCO_3$ aerosol heterogeneous chemistry in the lower stratosphere, the intended region of SAI application.[142] Therefore, it is essential to experimentally measure the uptake coefficients of relevant gases on $CaCO_3$ aerosol surface under stratospheric conditions.[243] Up until recently, there have been numerous studies on the heterogeneous reactions between $CaCO_3$ and NO_x reservoir species, such as HNO_3 (ref. 184 and 244–250) and N_2O_5,[251–254] at ambient conditions in the context of urban pollution. However, due to variations in experimental techniques and conditions, the uptake coefficients of HNO_3 and N_2O_5 on the surface of $CaCO_3$ particles vary over a few orders of magnitude, $10^{-5} < \gamma_{HNO_3} < 0.3$ and $10^{-4} < \gamma_{N_2O_5} < 0.1$, respectively (Table 2). Besides, only a few of those studies experimented with airborne $CaCO_3$ particles,[249,252,254] a technique that reduces experimental diffusion limitations and is a better representation of aerosols used in the case of SAI application than, *e.g.*, studying particles deposited on a surface. In addition, there are just two room temperature studies on the uptake of HCl, a ClO_x reservoir species, on $CaCO_3$ particles, where only Huynh and McNeill (2020) explored the reaction of $CaCO_3$ aerosols using an aerosol flow tube (AFT) coupled with a quadrupole chemical ionization mass spectrometer (CIMS).[184] Building upon the understanding of $CaCO_3$ heterogeneous chemistry at ambient conditions, two experimental studies were recently conducted at stratospheric temperature to further explore the gas uptake on $CaCO_3$ particles. Dai *et al.* (2020) performed experiments on a range of reactions at 200 K and 1.6 Torr with a coated-wall flow tube coupled with a CIMS. The authors determined both the HNO_3 and HCl uptake coefficient values on the surface of $CaCO_3$ layers to be very small, $\sim 10^{-5} < \gamma_o < 10^{-4}$ for initial uptake coefficients (γ_o) and $\sim 10^{-12} < \gamma_{ss} < 10^{-7}$ for steady-state uptake coefficients (γ_{ss}).[178] Huynh and McNeill (2021) derived the initial uptake of HCl on the surface of airborne $CaCO_3$ aerosols at 207 K and ambient pressure to be $\gamma_o \sim 0.076$,[263] at least three orders of magnitude higher. Again, the difference in experimental techniques may have contributed to the disparity in γ_o values. The measured gas uptake in Dai *et al.* (2020) may also have been inhibited by the diffusion limitations associated with a coated-wall AFT or by a residual organic coating on $CaCO_3$.[237,264] By using the same aerosol generation process and experimental method (AFT-CIMS) between their ambient and stratospheric studies, Huynh and McNeill (2021) also determined that the heterogeneous reaction between $CaCO_3$ aerosols and HCl gas proceeds more efficiently under stratospheric conditions.

3.1.3 Modeling of SAI ozone effects. Stratospheric O_3 depletion caused by substantial stratospheric aerosol burden has been extensively investigated using numerical simulations in several SAI scenarios using sulfate[81,89,102,175,265] and other aerosol materials.[86,142,143] Pitari *et al.* (2014) conducted a comprehensive study of sulfate SAI. The authors modelled the global O_3 response for different SO_2 injection scenarios, G3 and G4 of GeoMIP,[182] using two general circulation models, GISS-E2-R and MIROC-ESM-CHEM, and two coupled chemistry-climate

Table 2 Overview of experimentally measured reactive uptake coefficient (γ) of relevant stratospheric trace gases on various proposed SAI aerosols in the literature. Aerosol heterogeneous chemistry with these reservoir species of stratospheric O_3 catalytic loss cycles greatly affect the global O_3 column as discussed in Section 3

Aerosol	Sample type	Gas-phase species	RH[a] (%)	Temp. (K) [pressure][b]	Gas concentration (molecule cm^{-3})	Initial uptake coefficient (γ_o)	Experimental technique[c]	Ref.	Pub. year
α-Al_2O_3	Particle	$ClONO_2$	<5	195–230	(1–10) $\times$ 10^{-7} Torr	0.02	AFT-EIMS	235	1997
		HCl		[1.0 Torr]	(1–10) $\times$ 10^{-6} Torr				
Al_2O_3	Powder	HNO_3	<5	298	6.5 $\times$ 10^{10} to 1.3 $\times$ 10^{12}	0.13 $\pm$ 0.033	Knudsen-MS	247	2001
α-Al_2O_3	Powder	HNO_3	<5*	298, 295	n/a	(9.7 $\pm$ 0.5) $\times$ 10^{-5}	Knudsen-MS	255 and 256	2001
α-Al_2O_3	Powder	HNO_3	<5	296	10^{14}	(4 $\pm$ 1) $\times$ 10^{-8}	FTIR	257	2001
γ-Al_2O_3	Powder	HNO_3	<5*	298	1 $\times$ 10^{11} to 2 $\times$ 10^{13}	0.13 $\pm$ 0.02	Knudsen-MS/ DRIFTS	258	2004
TiO_2	Aerosol	N_2O_5	5 $\pm$ 1	296 $\pm$ 2	(1–5) $\times$ 10^{13}	[d] (1.2 $\pm$ 0.2) $\times$ 10^{-3}	AFT-CLD	259	2014
			23 $\pm$ 2			(0.7 $\pm$ 0.1) $\times$ 10^{-3}			
			45 $\pm$ 3			(1.5 $\pm$ 0.3) $\times$ 10^{-3}			
			60 $\pm$ 3			(3.0 $\pm$ 1.4) $\times$ 10^{-3}			
TiO_2	Aerosol	$ClONO_2$	7 $\pm$ 1	296 $\pm$ 2	1.7 $\times$ 10^{13}	1.2 $\times$ 10^{-3}	AFT-CLD	260	2016
			33 $\pm$ 3						
TiO_2	Aerosol	HO_2	11 $\pm$ 1	293 $\pm$ 3	1.6 $\times$ 10^{9}	[d] (2.1 $\pm$ 0.1) $\times$ 10^{-2}	AFT-FAGE	261	2018
			30 $\pm$ 1			(2.5 $\pm$ 0.2) $\times$ 10^{-2}			
			45 $\pm$ 1			(2.9 $\pm$ 0.5) $\times$ 10^{-2}			
			66 $\pm$ 1			(3.6 $\pm$ 0.7) $\times$ 10^{-2}			
$CaCO_3$	Powder	HNO_3	<5	298	10^{10} to 10^{13}	0.071	Knudsen-MS	244	1995
$CaCO_3$	Pellet	HNO_3	<5	298	10^{10} to 10^{13}	0.06	Knudsen-MS	244	1995
			>5			0.15 $\pm$ 0.03			
$CaCO_3$	Powder	HNO_3	<5	298	1 $\times$ 10^{11}	1.4 $\times$ 10^{-5}	Knudsen-MS	245	2000
$CaCO_3$	Powder	HNO_3	<5*	295	1 $\times$ 10^{12}	(2.5 $\pm$ 0.1) $\times$ 10^{-4}	Knudsen-MS DRIFTS	246	2000
$CaCO_3$	Powder	HNO_3	<5*	298	6.5 $\times$ 10^{10} to 1.3 $\times$ 10^{12}	[e] 0.10 $\pm$ 0.025	Knudsen-MS	247	2001
						[e] 0.18 $\pm$ 0.045			
$CaCO_3$	Powder	HNO_3	<5	296	6.5 $\times$ 10^{10}	(2 $\pm$ 1) $\times$ 10^{-3}	Knudsen-MS	248	2005
$CaCO_3$	Aerosol	HNO_3	33	296	10^{12}	0.11	AFT[b]-denuder	249	2006
$CaCO_3$	Powder	HNO_3	<5	300 $\pm$ 1	(3–7) $\times$ 10^{11}	0.3	Knudsen-MS	250	2006
$CaCO_3$	Particle	HNO_3	40	298	$\sim$(2–6) $\times$ 10^{11}	[f] 0.06	PS-SFR SEM/EDX	262	2008
			80			0.21			
$CaCO_3$	Particle	HNO_3	<5	298 $\pm$ 1	5.2 $\times$ 10^{10} to 7.8 $\times$ 10^{13}	0.013 $\leq \gamma_o \leq$ 0.14	Particle-FTIR	184	2020
$CaCO_3$	Layer	HNO_3	<5*	215 $\pm$ 2 [1.7 Torr]	n/a	(2.5 $\pm$ 1.8) $\times$ 10^{-4}	Coated-wall FT-CIMS	177	2020
$CaCO_3$	Powder	HCl	<5	300 $\pm$ 1	6 $\times$ 10^{11}	0.13	Knudsen-MS	250	2006
$CaCO_3$	Particle	HCl	<5	298 $\pm$ 1	7.0 $\times$ 10^{11} to 1.6 $\times$ 10^{14}	0.0011 $\leq \gamma_o \leq$ 0.012	Particle-FTIR	184	2020
$CaCO_3$	Aerosol	HCl	<5	298 $\pm$ 1	5.4 $\times$ 10^{12}	0.013 $\pm$ 0.001	AFT-CIMS	184	2020
$CaCO_3$	Layer	HCl	<5*	215 $\pm$ 2 [1.7 Torr]	7.2 $\times$ 10^{11}	(7.2 $\pm$ 5) $\times$ 10^{-5}	Coated-wall FT-CIMS	178	2020
$CaCO_3$	Layer	HCl	<5	200 $\pm$ 2	5.4 $\times$ 10^{14} to 3.6 $\times$ 10^{17}	[f] (3.0 $\pm$ 0.6) $\times$ 10^{-12} to (3.3 $\pm$ 0.6) $\times$ 10^{-7}	Flask-CIMS	178	2020
$CaCO_3$	Layer	HCl	<5*	298	n/a	[g] (9.8 $\pm$ 9) $\times$ 10^{-5}	Coated-wall FT-CIMS	178	2020
		$ClONO_2$		215 $\pm$ 2 [1.7 Torr]					
$CaCO_3$	Aerosol	HCl	<5	207 $\pm$ 3	3.6 $\times$ 10^{12}	0.076 $\pm$ 0.009	AFT-CIMS	263	2021
$CaCO_3$	Powder	N_2O_5	<5*	298 $\pm$ 2	(4.0 $\pm$ 1.0) $\times$ 10^{11}	0.12 $\pm$ 0.04	Knudsen-MS	251	2006
						[f] 0.021 $\pm$ 0.006			
$CaCO_3$	Aerosol	N_2O_5	<1	290	2.5 $\times$ 10^{15}	(1.9 $\pm$ 0.2) $\times$ 10^{-4}	Chamber-FTIR	252	2006
$CaCO_3$	Powder	N_2O_5	0*	296 $\pm$ 2	3 $\times$ 10^{9} to 2 $\times$ 10^{10}	[e] 0.026 $\pm$ 0.008	Knudsen-MS	253	2008
						[e] 0.05 $\pm$ 0.02			
$CaCO_3$	Aerosol	N_2O_5	0*	296 $\pm$ 2	(1–40) $\times$ 10^{12}	[h] (4.8 $\pm$ 0.7) $\times$ 10^{-3}	AFT-CLD	254	2009
						(5.3 $\pm$ 1.0) $\times$ 10^{-3}			

Table 2 (*Contd.*)

Aerosol type	Sample	Gas-phase species	RH[a] (%)	Temp. (K) [pressure][b]	Gas concentration (molecule cm^{-3})	Initial uptake coefficient (γ_o)	Experimental technique[c]	Ref.	Pub. year
			29 ± 2						
			58 ± 3			$(11.3 \pm 1.6) \times 10^{-3}$			
			71 ± 4			$(19.4 \pm 2.2) \times 10^{-3}$			

[a] Dry condition is denoted as RH (%) < 5 if not specified by the studies. If the sample was generated from aqueous slurry and then dried under vacuum, RH (%) < 5*. [b] Pressure is only specified for studies not conducted at ambient pressure. [c] A full list of experimental techniques are included at the end of the paper. [d] See the referenced papers for the full range of studied RH. [e] Heated and unheated powders that was previously mixed with ethanol. [f] Steady-state uptake coefficient. [g] $CaCO_3$ layers were exposed to HCl first for 8 h at room temperature before being exposed to $ClONO_2$. [h] The true uncertainty of the uptake coefficient values may be a factor of two to four due to particle shape assumption.

models, ULAQ-CCM and GEOSCCM.[102] Even though both scenarios have RCP4.5 (ref. 180) as the anthropogenic forcing profile, G3 involves periodic injections of SO_2 to keep the TOA net radiation constant, whereas G4 involves a constant injection of 5 Tg SO_2 annually. A summary of the study results is included in Table 1. During the simulated SAI period of 2020–2070, the global O_3 column was depleted at a slower rate over time for G4, as seen in Fig. 8a. Due to the estimated decline in stratospheric chlorine burden *via* the Montreal Protocol and the continued suppression of the NO_x cycle *via* (R4), global O_3 level was projected to recover over the SAI period. Unlike G4, G3 simulations predicted a steeper increase in global O_3 loss especially in the absence of aerosol heterogeneous chemistry (Fig. 8b). Fig. 8c depicts the varying latitudinal distributions of O_3 column anomaly for the decade 2040–2049, which was caused by the different assumptions in the models, such as aerosol heterogeneous chemistry, microphysics, and photolysis changes. For example, GISS-E2-R G4nhc simulated up to 15 DU reduction in the mid-latitudes due to the lack of NO_x cycle in the model to compensate for the photochemical O_3 depletion. On the other hand, other G4 simulations like ULAQ-CCM only predicted less than 5 DU reduction in the O_3 column. Despite the varying degrees of stratospheric O_3 depletion based on model parameters, this 2014 study like many other modeling studies[81,142,143,175,265] have modelled that sulfate SAI generally depleted the O_3 column regardless of SAI scenarios. The modelled negative effect on the stratospheric O_3 level is consistent with observations made following volcanic eruptions, as discussed previously. A recent modeling study by Visioni *et al.* (2021) and Tilmes *et al.* (2022) simulated the climate impacts of sulfate SAI against SSP5-8.5,[266] a projected high GHG emission scenario (Table 1).[107,179] The authors determined that changes to TCO are small (<20 DU) compared to the base case scenario of SSP5-8.5. However, the simulation required a continuous increase in SO_2 injection.[107] The associated risks of SAI like stratospheric O_3 depletion, as a result, may increase over time.

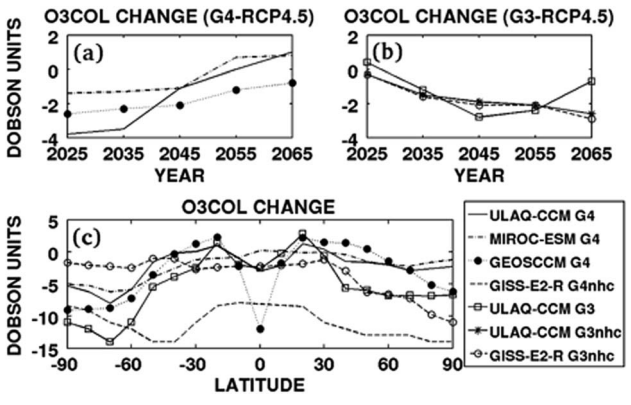

Fig. 8 Modeling simulations of global O_3 column changes in (a) G4 and (b) G3 with respect to the base case RCP4.5 over time. (c) Zonally and time-averaged column ozone changes (2040–2049). Reprinted with permission of the publisher from Pitari *et al., J. Geophys. Res.*, 2014, **119**, 2629–2653.

Al_2O_3 particles, a potential alternative to sulfate, had their impact on global O_3 levels explored by Weisenstein and co-authors (2015) *via* a 2-D chemistry-transport-aerosol model.[142] As seen in Fig. 9, for the range of tested Al_2O_3 particle sizes, between 80 nm and 240 nm in radius, coated or uncoated with existing aqueous sulfate in the stratosphere, there was significant O_3 depletion at middle and high latitudes in both hemispheres (~6–10%), albeit less than that caused by sulfate. The modelled O_3 loss scales inversely with the Al_2O_3 particle size, with 240 nm Al_2O_3 particles causing the least damage to the O_3 level compared to all tested aerosol materials, confirming that aerosol size is an important factor in designing SAI aerosol. Although the application of Al_2O_3 aerosols in SAI should be investigated more in depth in a 3-D transport model, this 2015 study suggests that Al_2O_3 particles of a suitable size may be able to limit damages to stratospheric O_3 compared to sulfate. The study also modelled the use of diamond particles, but, in addition to economic considerations, heterogeneous reactions on diamond have not been studied.

TiO_2 particles were experimentally studied then applied by Tang *et al.* (2014)[242] in their chemistry-climate model. The

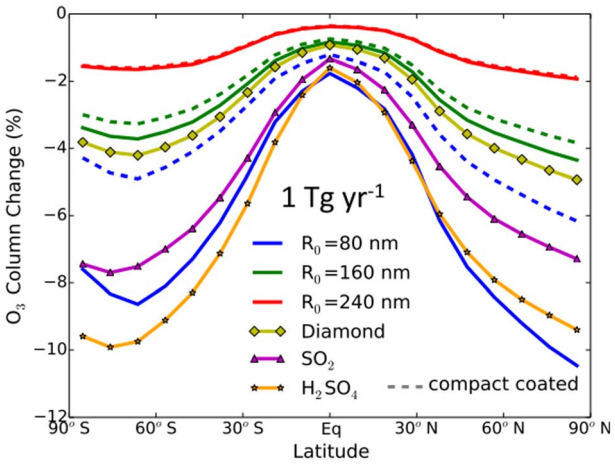

Fig. 9 Average O_3 column change per year as a function of latitudes with an annual injection rate of 1 Tg of Al_2O_3 monomers of 80 nm (blue), 160 nm (green), 240 nm (red), 160 nm diamond monomers (dark yellow), SO_2 (magenta), and H_2SO_4 (orange). Reprinted from Weisenstein *et al.*, *Atmos. Chem. Phys.*, 2015, **15**, 11835–11859. Distributed under a Creative Commons Attribution 4.0 License (CC BY 4.0) https://creativecommons.org/licenses/by/4.0/.

authors used a range of uptake coefficient values of N_2O_5 on TiO_2 particles, 0.001 to 0.005, where the lower limit was derived experimentally and the upper limited was estimated based on stratospheric conditions. N_2O_5 stratospheric concentration was projected to reduce by 30% in the presence of stratospheric TiO_2 particles compared to ~90% in the presence of Pinatubo's level sulfate aerosols. Heterogeneous chlorine activation on TiO_2 particles has not been studied experimentally and, therefore, was not included in the 2014 model. As a result, the impact of TiO_2 particles on stratospheric O_3 is still uncertain.

For $CaCO_3$ particles, commonly used as a proxy for mineral dust, Keith *et al.* (2016) analyzed the effects of stratospheric $CaCO_3$ injection on O_3 loss by investigating the perturbations of $CaCO_3$ heterogeneous chemistry to individual O_3 catalytic cycles. For a $CaCO_3$ injection rate of 5.6 Tg per year,[143] ~20% of the peak sulfate level post Pinatubo's eruption,[75] the fraction of total O_3 loss due to the NO_x cycle was drastically reduced by 10% in the lower stratosphere (~12–30 km), while that due to the other catalytic cycles, such as ClO_x, HO_x and BrO_x, became more prominent in the same region. These cycle shifts were consistent with the aerosol heterogeneous chemistry expressed earlier *via* (R1)–(R4). The annual average O_3 column increased by 6.4% in this $CaCO_3$ SAI scenario despite some O_3 loss in the lower stratosphere and upper troposphere, compared to the general O_3 loss caused by other studied materials including Al_2O_3, diamond, and sulfate. However, the authors only included $CaCO_3$ reactions with the following acidic gases: HCl, HBr, HNO_3, and H_2SO_4, using estimated mechanisms and rate coefficients in the aerosol transport model. The other important NO_x and ClO_x reservoir species, N_2O_5 and $ClONO_2$, respectively, whose reactions on aerosol surfaces disrupt stratospheric photochemical cycles and lead to ozone depletion (R1)–(R4), were not included in the 2016 modeling study. More importantly, there are uncertainties in that 2016 estimate of O_3 stratospheric chemical processes since there was little understanding of $CaCO_3$ aerosol chemical kinetics in the stratosphere at the time.

Following experimental studies of $CaCO_3$ heterogeneous chemistry under stratospheric conditions as summarized in Table 2, Dai and co-authors also modelled the impact of $CaCO_3$ heterogeneous chemistry on the O_3 column as shown in Fig. 10. A wide range of global O_3 column change, between −5% to +25%, was estimated based on various assumptions of trace gas uptake on $CaCO_3$ aerosols. Applying the HCl uptake coefficient determined in Huynh and McNeill (2021), there was estimated to be about 5% reduction in the O_3 column at the middle to high latitudes in the SH. Overall, additional experimental studies are needed to measure the uptake of stratospherically relevant gases on $CaCO_3$ aerosols under realistic SAI conditions. Nevertheless, coupled with a minimal rate of stratospheric heating (<0.2 K) as discussed in Section 2, the potentially limited stratospheric O_3 loss makes $CaCO_3$ a promising alternative compared to other proposed aerosols.

3.2 Tropospheric ozone

Tropospheric O_3 level is controlled by STE, atmospheric water vapor level, and the following reaction sequence as summarized by Xia *et al.* (2017).

$$NO_2 + h\nu\ (\lambda < 420\ \text{nm}) \rightarrow NO + O(^3P) \quad \text{(R5)}$$

$$O(^3P) + O_2 + M \rightarrow O_3 + M \quad \text{(R6)}$$

Tropospheric O_3 production is driven by NO_2 photolysis followed by a three-body reaction (R5) and (R6). NO_2 production

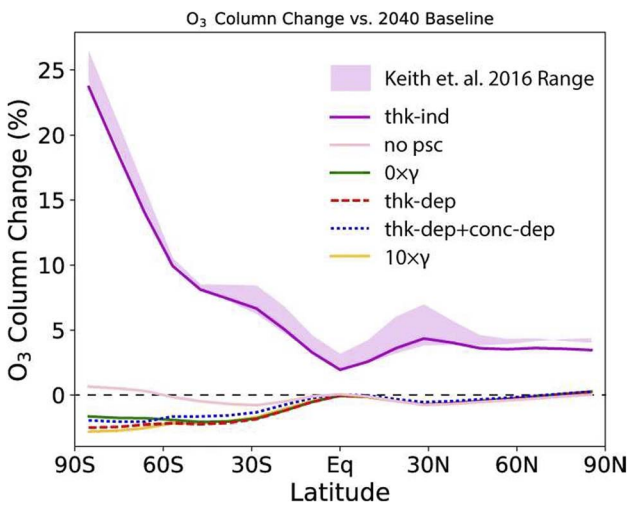

Fig. 10 O_3 column change compared to the 2040 baseline under various assumptions of $CaCO_3$ aerosol heterogeneous chemistry measured in a coated-wall flow tube coupled with a CIMS (Table 2). The gas uptake coefficients were calculated both dependently (denoted with thik-dep) or independently (thik-ind) of $CaCO_3$ layer thickness. Reprinted from Dai *et al.*, *Commun. Earth Environ.*, 2020, **1**, 1–9. Distributed under a Creative Commons Attribution 4.0 International License (CC BY 4.0) https://creativecommons.org/licenses/by/4.0/.

depends on the oxidation of NO by reaction with peroxy radicals in the atmosphere (*e.g.*, (R7) and (R8)) where R represents a generic organic group such as CH_3.

$$HO_2 + NO \rightarrow NO_2 + OH \quad (R7)$$

$$RO_2 + NO \rightarrow NO_2 + RO \quad (R8)$$

RO_2 is produced *via* oxidation of volatile organic compounds (VOCs) with OH which is formed *via* O_3 photolysis and the subsequent reaction with tropospheric H_2O vapor (R9) and (R10).

$$O_3 + h\nu\ (\lambda < 320\ \text{nm}) \rightarrow O(^3P) + O_2 \quad (R9)$$

$$O(^1D) + H_2O \rightarrow 2OH \quad (R10)$$

Since the global surface temperature is cooled across all SAI scenarios, we expect tropospheric H_2O vapor concentration to decrease with reduced solar radiation,[128] which in turn slows down OH production as well as O_3 loss *via* (R10) and (R9), respectively. Furthermore, since stratospheric O_3 is very likely depleted as discussed previously in Section 3.1, more UV radiation could reach the troposphere and increase the rates of photochemical reactions, affecting both O_3 production (R5) and O_3 consumption (R9).[267,268]

Following Mt. Pinatubo's eruption, tropospheric O_3 level was observed to decline significantly at both middle and high latitudes in 1992 and 1993.[269,270] Tang *et al.* (2013) speculated that the tropospheric O_3 decrease was largely driven by a significant reduction in the STE of O_3, at a maximum of about −70 Tg per year in January 1993 (Fig. 11a).[88] The decline in the global mean tropospheric O_3 column peaked at 1.9 DU in November 1992 as illustrated in Fig. 11b. The change in O_3 STE is driven by changes in either stratospheric O_3 concentration or the strength of the BDC that is responsible for the exchange of air masses between the stratosphere and the troposphere. As seen in Fig. 11c, there is no statistically significant difference in the global downward air mass flux at 100 hPa after the volcanic eruption, further reinforcing that stratospheric O_3 depletion was mainly responsible for the decrease in the O_3 STE. An increase in tropospheric photochemical O_3 production in 1991–1995 was estimated to compensate for ~67% of the decrease in the O_3 STE flux. As a result, O_3 level was projected to go up in some tropical regions.[88] This regional increase in surface level O_3 is consistent with TOMS data from the period of 1979–1995.[270]

For the SAI simulation of injecting 8 Tg per year of sulfate aerosols over a 50 year period (Table 1), Xia *et al.* (2017) also reported a global reduction in surface O_3 level except with a regional increase in the tropics across all latitudes.[89] In this study the dominant pathway was determined to be the reduction of H_2O vapor in the atmosphere, accounting for ~90% of the overall reduction in O_3 loss. The reduction in tropospheric O_3 loss dominated in the tropics and thus led to an increase in surface O_3 level there (+1.2 ppb), while the reduced STE of O_3 dominated at middle to high latitudes, resulting in surface O_3 decrease (−1.6 ppb). The regional differences in surface O_3 concentration are due to characteristics of SAI simulation (injection location, frequency, *etc.*) As an air pollutant and a GHG, both potential increases and decreases in tropospheric and surface O_3 should be considered in future SAI research planning and deployments.

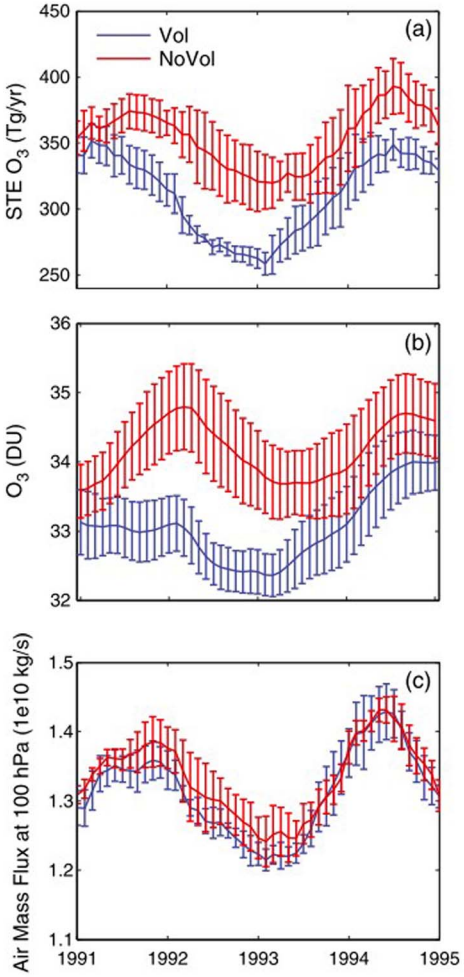

Fig. 11 12 Month running means of global (a) STE O_3 fluxes, (b) tropospheric O_3 columns, and (c) downward air mass fluxes at 100 hPa for the period of 1991–1995 for both volcanic (Vol) and non-volcanic (NoVol) scenarios. Reprinted with permission of the publisher from Tang *et al.*, *Geophys. Res. Lett.*, 2013, **40**, 5553–5558.

4 Other climate effects

4.1 Hydrological cycle

As global warming continues due to the projected increase in anthropogenic emissions of CO_2 in the next few decades, atmospheric moisture content is expected to increase due to higher evaporation rate, leading to an enhancement in precipitation rates. The predicted rise in both heavier rainfalls and their frequency may increase the risk of flooding especially over the monsoonal regions.[271–273] It is, therefore, important to investigate to what extent climate geoengineering proposals such as SAI would influence the hydrological cycle.[156,274–276] Trenberth *et al.* (2007) investigated the hydrological response to

previous major volcanic eruptions with a special focus on Mt. Pinatubo's eruption (June 1991). According to historical records, from October 1991 to September 1992 the land precipitation was about three standard deviations below normal, while the river discharge into the oceans was almost four standard deviations below normal.[153] The record decrease in precipitation and thus freshwater sources imply a potential risk for widespread drought in SAI scenarios. In fact, Haywood *et al.* (2013) suggested that the volcanic eruptions in the NH contributed significantly to the Sahelian drought in the 1970–1990s.[275] In 2015, Iles and Gerberl[277] also detected significant regional differences in the streamflow volume of large rivers globally following explosive eruptions, prompting additional research on the regional hydrological responses to SAI. In a 2019 study, Simpson and co-authors[180] explored the hydroclimate responses for different regions across the globe by simulating sulfate SAI under the most severe forcing scenario, RCP8.5 (Table 1). Fig. 12 below from their study illustrates the projected precipitation changes from offsetting the increase in global mean surface temperature over many 20 year periods starting in 2020 until 2095.

As illustrated in Fig. 12, there seems to be a linear correlation between the negative precipitation change and the globally averaged temperature anomalies[278] for most regions. Since the study assumes that SAI is required to offset more global warming over time, the modelled areas are projected to get drier with a steeper reduction in precipitation. However, there are exceptions in the following regions: Amazonia in the summer (JJA) (Fig. 13c), West Australia and Mediterranean in the winter (DJF) (Fig. 12g and k). The reason for these exceptions is currently unclear. The study also observed that stratospheric heating in the tropics, which was caused by the significant loading of stratospheric sulfate aerosols as discussed previously in Section 2, reduced precipitation in regions of climatologically high precipitation, including monsoonal regions such as central India. Despite uncertainties (*e.g.*, precipitation biases) in the 2019 model, the projected trend of reduced precipitation over most of the globe from the application of SAI is consistent with historical observations after volcanic eruptions. Besides stratospheric warming, there are also additional mechanisms that could be responsible for changes in the hydrological cycle, including the aerosol–cloud interactions as covered in Section 2. Overall, depending on the SAI scenarios, changes to both global and regional hydrological cycles could vary and, therefore, this is an active research area of SAI modeling studies.[270]

4.2 Tropical cyclones

In addition to the hydrological cycles, other climate effects of SAI application have been explored, notably how it would affect extreme weather events such as tropical cyclones (TC) and hurricanes.[176,279,280] Irvine *et al.* (2019) determined that the global warming caused by a two-fold increase of CO_2 over a 130 year period would be halved, if the solar constant is reduced by 1% by SAI over the same period.[280] Not accounting for stratospheric aerosol chemistry, Irvine *et al.* simulated that SAI in this case offset most of the increase in TC intensity with <0.4% of land surface experiencing climate risks such as extreme precipitation. Other modeling studies have determined that volcanic eruptions could shift the Intertropical convergence zone (ITCZ) which, coupled with the change in surface temperature, affects TC activity.[176,279,281] Applying that hypothesis to SAI applications, Moore *et al.* (2015)[279] estimated that for both G3 and G4 scenarios of GeoMIP[182] stratospheric sulfate aerosol loading ameliorated the intensity and frequency of Atlantic hurricanes as well as reduced coastal floor risk during the SAI simulated period (Table 1). Nevertheless, there was no clear evidence that SAI would be able to mitigate the predicted increase in storm surge events as severe as Hurricane Katrina (2005) under RCP4.5 scenario. Similarly, Jones *et al.* (2017)[176] also estimated how SAI would affect North Atlantic TC frequency and intensity compared to the same base case (RCP4.5) with a general circulation model (GCM). In addition to simulating a relatively uniform global distribution of stratospheric sulfate aerosols (G4), the 2017 paper also studied the impacts on TCs of regional SAI applications, specifically in the NH (G4NH) and in the SH (G4SH) (Table 1) using three different approaches. First, by training the model with historical TC observations, the model predicted a significant reduction in the North Atlantic storm frequency (TCs per year) for G4NH scenario, consistent with observations of attenuated TC activity after the eruptions of Mt. Pinatubo and El Chíchon.[282,283] On the other hand, G4SH was predicted to increase the storm frequency by more than 50% over the 50 year SAI period. G4 was also modelled to increase the numbers of TCs per year but not significantly (<20%). The model also yielded relatively similar predictions when simulated with meteorological parameters known to affect TC activity, including wind shear over the main storm development region, precipitation, and relative sea surface temperature.[284–286] Lastly, by employing a downscaling model the authors investigated not only the frequency but also the intensity of different storm categories (TC, hurricanes, and major hurricanes) as illustrated in Fig. 13.

This statistical-dynamical downscaling algorithm predicted an increasing trend for TC activity for the base case scenario, RCP4.5, compared to the stable trend from the previous two approaches. The disparity between a downscaling simulation and the previous two GCM simulations have also been observed in other studies, and origin of the discrepancy remains unclear.[287–289] The third simulation also projected that all SAI scenarios lowered the storm frequency during the entire SAI period, with G4 and G4NH having the strongest reduction capability (up to 50%). Despite the varying results across three simulations during the SAI implementation period, immediately after SAI was abruptly stopped the numbers of TCs were all modelled to return to the base case level over a 20 year period. Despite the positive predictions of both the 2015 and 2017 models on SAI's ability to reduce the frequency and intensity of TCs, they both focused on the Northern Atlantic region only. A recent study by Pausata and Camargo (2019)[281] suggested that volcanic eruptions do not reduce TC activity but rather redistribute the TCs globally, prompting similar research before we could ascertain SAI true impact on such extreme weather events. Additionally, future studies should consider the likely

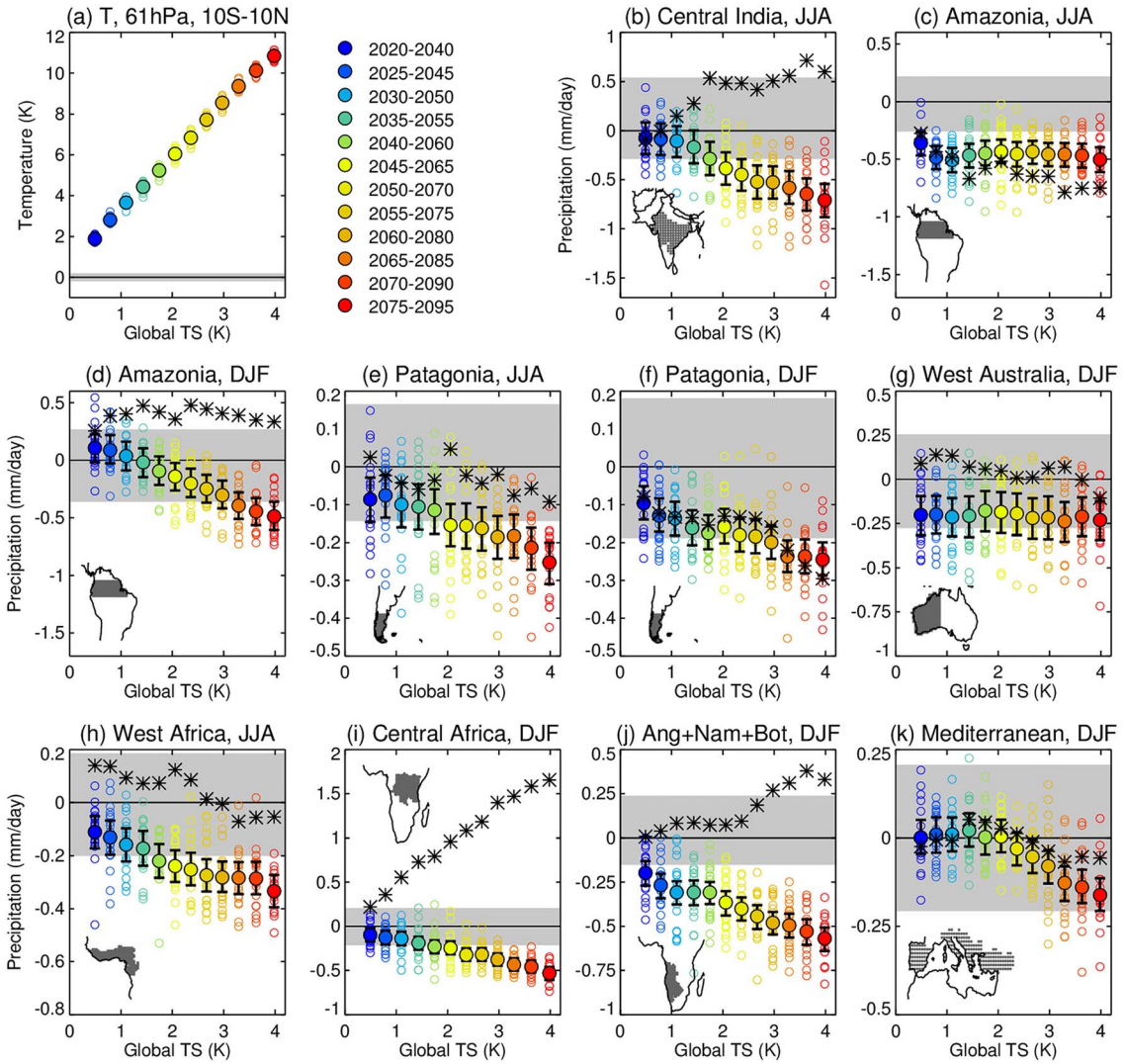

Fig. 12 (a) Zonal mean stratospheric temperature at 61 hPa. (b)–(k) Precipitation anomalies as a function of globally averaged temperature anomalies (RCP8.5-BASE), where RCP8.5 represents years 2075–2095 of a three-member ensemble run from 2010 to 2099 under RCP8.5 forcings and BASE are 2010–2030 simulations under RCP8.5 forcings. The illustrated regions were all modelled to sustain significant drying. Reprinted with permission of the publisher from Simpson *et al.*, *J. Geophys. Res. Atmos.*, 2019, **124**, 12587–12616.

difference between regional and global SAI applications on other extreme weather events (*e.g.*, heat waves).

4.3 Biodiversity

As a general threat to biodiversity, global warming has been determined to elevate sea surface temperatures, that in turn has caused widespread coral bleaching.[290–292] In addition, the rapid rise in global CO_2 levels has led to an unprecedented rate of ocean acidification, further destroying the coral communities *via* calcification.[293,294] Besides coral reefs, other marine and terrestrial biodiversity are also at risk of extinction since they are estimated to not be able to adapt to the rapid rate of climate change.[295,296] Trisos *et al.* (2018)[297] explored the impacts of SAI implementation on a variety of global biodiversity hotspots by modeling their climate velocities, specifically the rate of change in precipitation and temperature in km per year (Fig. 14). Defined as the rates and directions that isotherms shift over time, the velocity of climate change has been demonstrated to be a good predictor of the geographical shifts of both marine and terrestrial species.[298–302] As illustrated in Fig. 14, Trisos and co-authors simulated the temperature velocities for different climate scenarios, including the global SAI scenario GeoMIP G4 over a 50 year geoengineering period, 2020–2069, and its 10 year sudden termination period starting in 2070. Fig. 14a highlights that most of the world's biodiversity hotspots are in the tropics, a region that has been predicted to suffer significant climate change effects such as increasing intensity of the hydrological cycle.[156,271,272,274] During G4 implementation, terrestrial species were modelled to sustain decreasing precipitation (Fig. 14b) and almost stable temperature across all studied categories (amphibians, birds, mammals, and reptiles) as shown in Fig. 14d. The reduction in climate velocities for land species once climate geoengineering is implemented compared to the

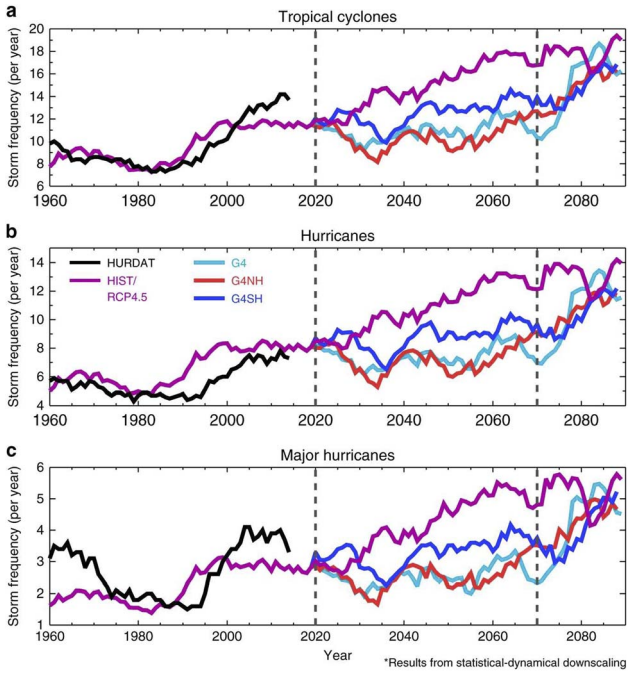

Fig. 13 Storm frequencies were modelled with a statistical dynamical downscaling method. (a) North Atlantic tropical cyclones (max windspeed > 20 m s^{-1}), (b) hurricanes (max windspeed > 37 m s^{-1}), and (c) major hurricanes (max windspeed > 96 m s^{-1}) were simulated for both the SAI 2020–2070 period and the period after SAI was stopped abruptly (2070–2090). HURDAT is the historical observations of storm tracking for 1960–2014, while RCP4.5 represents the base case scenario. G4 is a global SAI scenario, whereas G4NH and G4SH are hemisphere-specific SAI scenarios. More simulation details and results are included in Table 1. Reprinted from Jones *et al., Nat. Commun.*, 2017, **8**, 1–10. Distributed under a Creative Commons Attribution 4.0 International License (CC BY 4.0) https://creativecommons.org/licenses/by/4.0/.

base case RCP4.5 signifies a mitigation to the warming-induced habitat migration. The first decade of implementing G4 has an even stronger effect on tropical marine species (corals, fish, and mangroves) with considerable negative temperature velocities (Fig. 14c). However, during the next 40 year G4 continuation period, the climate velocities for all species return to the same levels as those of RCP4.5, implying that G4 only provides a short-term relief to the climate change effects on the biodiversity hotspots. Once G4 is terminated in 2070, the marine and terrestrial species over the next decade were predicted to experience extreme temperature velocities that are 2–4 times higher than both historical trends and RCP4.5 scenario. Especially poorly dispersing species, such as corals and amphibians, were modelled to be at an increased risk of extinction in the scenario of SAI sudden termination, as they would be due to climate change.[303] SAI modelling studies have looked at how different SAI implementation schemes may impact the environment.[109,136] As a result, it is unlikely for SAI implementation to be terminated abruptly given its negative effect as pointed out in this study. Regardless, it is important to note that SAI has the ability to negatively affect the global biodiversity hotspots even more than the rapid rise in GHGs concentrations, if not designed properly.

5 Governance and economics

Any successful application of SRM would, by design, impact the climate and ecosystems of multiple nations. Therefore, multinational cooperation and agreement should be sought out before such a deployment.[304] The National Academies of Sciences, Engineering, and Medicines reported in their 2021 study[305] that almost one thirds of all geoengineering studies from 1983 to 2020 was on governance, economics or social sciences. However, there is limited diversity both in the research community for solar geoengineering and in relevant public engagement.[306–308] In addition, there is still little to no governance and economic frameworks in place as summarized by Flegal *et al.* (2019).[309] Such frameworks would entail guidelines and regulations regarding the scope and responsibility of SRM research, including regional and global deployment and maintenance. In 2019, MacMartin and co-authors[310] examined the technical dimensions of an SAI deployment that will most likely affect the on-going decisions of whether to continue SAI and, if so, how to continue. The study suggested that some SAI uncertainties could be managed *via* a feedback system as demonstrated in previous modeling studies.[311–314] For example, the amount of aerosol injection needed could be adjusted during the SAI implementation process based on how much of the 'observed' global mean temperature we aim to offset.[314] However, before SAI application there are still several important questions that lack a systematic response, including the following: who should decide when and where the SAI deployment should be? Who will be paying for the research cost, initial and ongoing deployment cost? What is the termination plan? Who will shoulder the compensation costs in the scenario that SAI causes unexpected major health or environmental impacts? *Etc.* A detailed review of ethical aspects of SRM has previously been covered by Preston *et al.* (2013), where potential concerns regarding different stages of SRM was analyzed.

The potential impacts of SRM deployment are estimated to be most severe for communities vulnerable to climate change, such as coastal areas and those around the tropics.[305] Within the past decade, Solar Radiation Management Governance Initiative (SRMGI), now known as the DEGREES (DEveloping Governance REsearch and Evaluation for SRM) Initiative, has administered grants to teams of 21 developing countries to research the impacts of SRM on their respective communities.[315] So far, this NGO funding effort has facilitated modeling studies of SAI regional impacts on climate extremes (*e.g.*, droughts)[316–318] and health risks[319] in Africa, the Middle East, and Southeast Asia to name a few.

In terms of governance, there have been proposals attempting to establish a hypothetical framework to govern the SRM process, including but not limited to research, aerosol production, deployment, and ongoing maintenance.[320–324] The general consensus is the need to expand SRM research beyond North American and European institutions and to begin assessing the possibility and applicability of SRM through

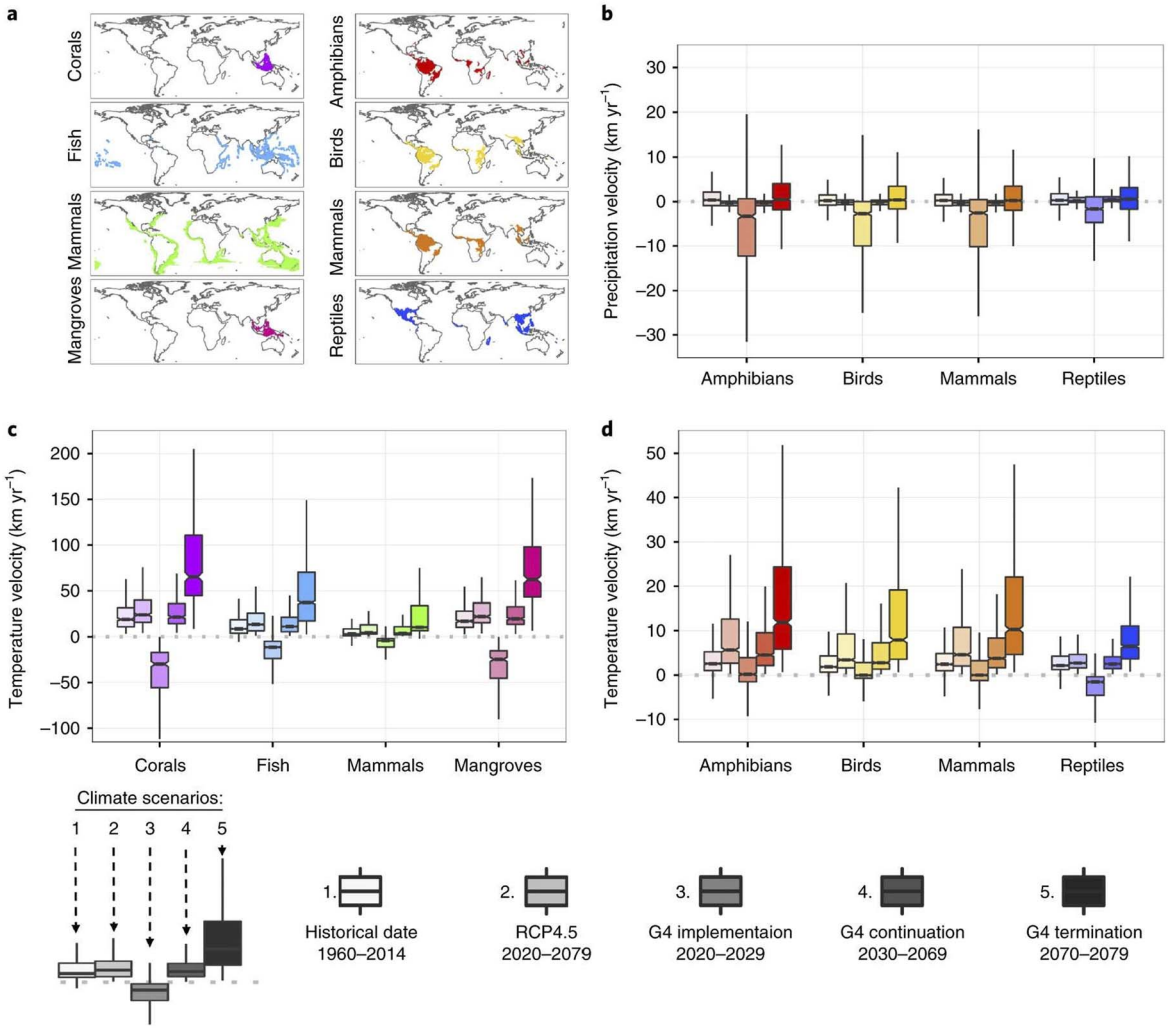

Fig. 14 Climate velocities for global diversity hotspots for different climate scenarios. (a) The locations represent the top 10% most species-rich areas where a given taxonomic group is found. (b) Precipitation velocities for terrestrial biodiversity hotspots. Temperature velocities for (c) marine biodiversity hotspots and (d) terrestrial biodiversity hotspots. Reprinted with permission of the publisher from Trisos *et al.*, *Nat. Ecol. Evol.*, 2018, **2**, 475–482.

a formally established governance.[305] It has been suggested that SRM or SAI research should be restricted to only numerical modeling and laboratory studies until multinational governance is established and adequate public outreach has been made.

Previously two preliminary SAI outdoor experiments were proposed and unsuccessfully attempted: the Stratospheric Particle Injection for Climate Engineering (SPICE) study and the Stratospheric Controlled Perturbation Experiment (SCoPEx). Mainly funded by the UK Engineering and Physical Sciences Research Council (EPSRC), the SPICE study had to postpone their first field trial in 2011 to spray H_2O at 1 km altitude due to backlash from NGOs and environmental groups.[325] In 2021, the first ScoPEx dry run in Sweden to test their instruments platform without injecting any particles received major pushbacks from local environmental groups as well as the indigenous community.[326] Despite having created an independent advisory board, ScoPEx has received general backlash including an open petition[327] signed by global environmental groups prior to their first attempt at outdoor experiments. In general, SAI research field experiments may continue to face scrutiny in the absence of international agreements and oversight.

Besides governance, the potential costs regarding implementation and maintenance of SAI have also been discussed in a few comprehensive studies.[328–330] McClellan and Keith *et al.* (2012) determined that there is existing technology capable of delivering millions of tons of SO_2 to the stratosphere. The authors estimated that it would cost about $5–8 billion annually to use new aircraft designs or ~$5 billion per year to use Boeing 747 Class airplanes to deliver 5 Mt of SO_2 annually to an altitude range between 20 and 30 km. This SAI implementation was estimated to zero out the anticipated increase in RF over a 50 year period starting in 2012.[328] Smith and Wagner (2018) also recommended an aircraft-based aerosol delivery system. Yet they concluded that existing technologies either could not reach the required altitude of at least 20 km (*e.g.*, military, or

commercial transport aircraft) or are too expensive to use (*e.g.*, NASA's high-altitude aircrafts). Including all development and operating costs, the 2018 study evaluated that about $2.25 billion per year is needed to inject ~0.2 Mt of SO_2 yearly starting in 2033 over a 15 year period to halve the projected global warming caused by anthropogenic GHG emissions.[330] Nonetheless, none of the studies so far included the costs of monitoring and measuring the impacts of SAI application and any other indirect costs, suggesting it to be at the lower end of the true costs. In addition, the estimates did not consider potential costs of remediation associated with possible unintended consequences of SAI implementation. Overall, SAI implementation and maintenance costs are functions of the designed scenario, including the duration, aerosol injection amount as well as injection location.

6 Conclusions and future research

Since its conception until today, SAI has prompted advanced modeling studies, many of which fully coupled different climate processes, including atmosphere, ocean, and land surface models. However, model simulations are necessarily limited in complexity compared to the real atmosphere and may not predict unintended consequences if the process in question is not represented in the model. Models necessarily involve many assumptions about poorly constrained processes such as aerosol microphysics and stratospheric chemistry.[105,106] For example, the refractive indices of many solid aerosols, the main alternatives to commonly studied sulfate aerosols, were empirically calculated,[161] reflecting uncertainties in the estimates of solid aerosols' radiative effects on both the level of stratospheric heating and changes in stratospheric water vapor.[82,140] The injected aerosol size and their temporal evolution (*e.g.*, *via* coagulation), despite being included in many modeling studies as listed in Table 1, have only been considered in the context of their radiative effects. The chemical evolution of injected aerosols over its stratospheric lifetime have not been accounted for, even though the aerosol size, especially surface area density, will inevitably transform due to the saturation of products on the aerosol surface upon reacting with traces gases[250] in the stratosphere. Therefore, the radiative impacts of aerosols require further research, especially because the extent to which aerosols could influence the Earth's albedo dictates the characteristics of SAI deployment, including aerosol injection rate, frequency, location as well as SAI implementation duration.[62,280,331]

Besides uncertainties about aerosol microphysics, so far few lab experiments have been conducted to characterize the stratospheric chemistry of proposed SAI aerosols,[178,184,259,263] most of which have only been studied at ambient conditions as summarized in Table 2. Aerosol heterogeneous chemistry with stratospheric NO_x and ClO_x reservoir species (*e.g.*, HNO_3, N_2O_5, and HCl) greatly affects global O_3 level as discussed in Section 3, and thus should be experimentally measured to provide reliable kinetic data for SAI modeling studies. As seen in Table 2, the wide range of measured gas uptake on aerosol surface, for example $CaCO_3$, is a result of not only by the various experimental techniques but also assumptions about the available aerosol surface area. Measurements involving airborne aerosol instead of powder provide a more accurate representation of the available surface sites for gas uptake upon aerosol release in the stratosphere. Our stratospheric temperature study of HCl uptake on airborne $CaCO_3$ aerosols with AFT-CIMS[263] sets up a good standard for other low-temperature experimental studies of aerosol heterogeneous chemistry. However, our current experimental technique is only applicable of measuring the initial gas uptake on aerosol surface. It is also essential to measure long-term gas uptakes to derive stratospheric lifetime of the studied aerosol. Dai *et al.* (2020) is the first study to measure long-term HCl uptake on the surface of $CaCO_3$ powder.[178] However, there are diffusion limitations when using a flask or a coated-wall flow tube technique as in their experiments, suggesting uncertainties with the results. Water plays an important role in increasing the reactivity of $CaCO_3$ aerosols and this should be explored under stratospheric conditions. Nevertheless, since there is only a trace amount of water in the lower stratosphere, 4×10^{-4} Torr H_2O vapor,[194] we do not expect a significant increase in gas uptake by $CaCO_3$ aerosol.

Together with the stratospheric chemical effects, downstream processes once the injected aerosols are transported to the troposphere, such as aerosol–cloud interactions and gravitational settling, have been projected to induce major climatic effects notably on the hydrological cycles,[156,274,276] extreme weather events,[62,176,279] and biodiversity[297,332] at both regional and global levels (Section 4). Although there are uncertainties in the modeling results due to variations in model parameters (*e.g.*, aerosol size distribution, stratospheric transport, *etc.*),[106,333] SAI was often determined to offset the negative impacts of climate change. Nevertheless, some studies projected that the abrupt termination of SAI would result in far more detrimental effects on the climate than the rise in anthropogenic GHGs emissions[334,335] (*e.g.*, biodiversity loss),[297] assuming no reduction in projected GHGs concentrations were made during the SAI period. Additionally, other studies such as Proctor *et al.* (2018) speculated that even the implementation of SAI provided little to no relief to the anticipated heat-induced stress on global agriculture from climate change.[177]

In addition to climate effects, there are also uncertainties about public health impacts of SAI aerosols. Effiong and Neitzel (2016)[336] characterized both occupational and public exposures to different SAI materials, including sulfate and alternatives (*e.g.*, BC, Al_2O_3, *etc.*). The study suggested that adverse health impacts are anticipated considering inhalation of suspended particles coupled with digestion of sedimented particles in water and food sources.[337–339] Since the toxicity of many of these aerosols are not well-studied and some of them are not routinely measured in the ambient atmosphere, the public exposure limits have not been formally established.

Overall, various SAI modeling studies over the past few decades have projected an array of climate and social impacts, intended and unintended. To minimize uncertainties associated with SAI, the chemical kinetics of proposed aerosols under stratospheric conditions need to be explored experimentally. Concurrently, atmospheric models should account for both physical and chemical evolutions of aerosols over its stratospheric lifetime to improve the modeling estimates of

stratospheric aerosol loading impacts particularly on cirrus clouds,[164,340] stratospheric water vapor and transport,[102,128] stratospheric temperature, and ozone chemistry.[89,102,142,143,178,265] Questions such as how to measure SAI impacts regionally and globally, how to dynamically adjust SAI parameters as a result of its observed effects, or how to terminate SAI, have been considered but remain open.[105,314] Addressing these concerns systematically should assist in setting up a multinational governance framework on scientific research, SAI deployment and termination scenarios, all of which are crucial to reliably consider SAI as a formal option to battle climate change.

Abbreviations

AASE II	Airborne arctic stratospheric experiment-II
AER-2D	Atmospheric and environmental research inc. 2D model
(CCM) SOCOLv2.0	Chemistry climate model solar climate ozone links version 2.0
AFT	Aerosol flow tube
AOD	Aerosol optical depth
BC	Black carbon
BDC	Brewer–Dobson circulation
CCN	Cloud condensation nuclei
CCT	Cirrus cloud thinning
CFCs	Chlorofluorocarbons
CIMS	Chemical ionization mass spectrometer
CLD	Chemiluminescence detector
FAGE	Fluorescence assay by gas expansion
DRIFTS	Diffuse reflectance infrared Fourier transform spectroscopy
DU	Dobson unit
ECHAM5-HAM	Fifth-generation atmospheric general circulation model
EIMS	Electron ionization mass spectrometer
ENSO	El Niño-Southern Oscillation
FTIR	Fourier transform infrared spectroscopy
GeoMIP	Geoengineering model intercomparison project
GEOSCCM	Goddard earth observing system chemistry climate model
GHG	Greenhouse gas
GISS ModelE2	NASA's Goddard institute for space studies model E2
IGCM	University of reading intermediate general circulation model
IPCC	Intergovernmental panel on climate change
ITCZ	Intertropical convergence zone
LW	Longwave
MCB	Marine cloud brightening
MIROC-ESM-CHEM	Earth system model based on model for interdisciplinary research on climate
MPI ESM	Max Planck institute earth system model
NDC	Nationally determined contributions
NH	Northern hemisphere
PSCs	Polar stratospheric clouds
PS-SFR	Particle-on-substrate stagnation flow reactor
RCP	Representative concentration pathway
RF	Radiative forcing
QBO	Quasi-biennial oscillation
RFG	Radiative forcing geoengineering
SAG	Surface albedo geoengineering
SAGE-II	Stratospheric aerosol and gas experiments-II
SAI	Stratospheric aerosol injection
ScoPEx	Stratospheric controlled perturbation experiment
SEM/EDX	Scanning electron microscopy/energy-dispersed X-ray spectrometer
SH	Southern hemisphere
SPICE	Stratospheric particle injection for climate engineering
STE	Stratosphere–troposphere exchange
SRM	Solar radiation management
SW	Shortwave
SWV	Stratospheric water vapor
TC	Tropical cyclones
TOA	Top-of-atmosphere
TOMS	Total ozone mapping spectrometer
TTL	Tropical tropopause layer
UHI	Urban heat islands
WACCM3	Whole atmosphere community climate model version 3
ULAQ-CCM	University of L'Aquila climate-chemistry coupled model
HadGEM2	Hadley center global environment model version 2
RRTM	Rapid radiative transfer model
CESM CAM4-chem	Community earth system model-community atmospheric model 4
CNRM-ESM2-1	Centre national de recherches meteorologiques earth system model of second generation
ISPL-CM6A-LR	Institut Pierre-Simon Laplace climate model for CMIP6-low resolution
UKESM1-0-LL	U.K. earth system model

Author contributions

All authors wrote and edited the paper.

Conflicts of interest

The authors declare there are no conflicts of interest.

Acknowledgements

The authors gratefully acknowledge the Eutopia Foundation for support of this work and for the reviewers for the careful review of the paper.

References

1 IPCC, *Climate Change 2014: Synthesis Report. Contribution of Working Groups I, II and III to the Fifth Assessment Report of*

the Intergovernmental Panel on Climate Change, IPCC, Geneva, Switzerland, 2014.
2 IPCC (Intergovernmental Panel on Climate Change), *Climate Change 2013: The Physical Science Basis*, Cambridge University Press, Cambridge, United Kingdom, 2013.
3 USGCRP (U.S. Global Change Research Program), *Climate Science Special Report: Fourth National Climate Assessment, Volume I*, 2018, vol. 1.
4 D. Habeeb, J. Vargo and B. Stone, *Nat. Hazards*, 2015, **76**, 1651–1665.
5 *IPCC, 2012: Managing the Risks of Extreme Events and Disasters to Advance Climate Change Adaptation. A Special Report of Working Groups I and II of the Intergovernmental Panel on Climate Change*, ed. C. B. Field, V. Barros, T. F. Stocker, D. Qin, D. J. Dokken, K. L. Ebi, M. D. Mastrandrea, K. J. Mach, G.-K. Plattner, S. K. Allen, M. Tignor and P. M. Midgley, Cambridge University Press, Cambridge, UK and New York, NY, USA, 2012.
6 R. J. Millar, J. S. Fuglestvedt, P. Friedlingstein, J. Rogelj, M. J. Grubb, H. D. Matthews, R. B. Skeie, P. M. Forster, D. J. Frame and M. R. Allen, *Nat. Geosci.*, 2017, **10**, 741–747.
7 P. Goodwin, A. Katavouta, V. M. Roussenov, G. L. Foster, E. J. Rohling and R. G. Williams, *Nat. Geosci.*, 2018, **11**, 102–107.
8 K. B. Tokarska and N. P. Gillett, *Nat. Clim. Change*, 2018, **8**, 296–299.
9 J. Rogelj, M. Den Elzen, N. Höhne, T. Fransen, H. Fekete, H. Winkler, R. Schaeffer, F. Sha, K. Riahi and M. Meinshausen, *Nature*, 2016, **534**, 631–639.
10 S. Fujimori, X. Su, J. Y. Liu, T. Hasegawa, K. Takahashi, T. Masui and M. Takimi, *Springerplus*, 2016, **5**, 1–11.
11 H. Benveniste, O. Boucher, C. Guivarch, H. Le Treut and P. Criqui, *Environ. Res. Lett.*, 2018, **13**, 14022.
12 Y. N. Ou, G. Iyer, L. Clarke, J. Edmonds, A. A. Fawcett, N. Hultman, J. R. McFarland, M. Binsted, R. Cui, C. Fyson, A. Geiges, S. Gonzales-Zuñiga, M. J. Gidden, N. Höhne, L. Jeffery, T. Kuramochi, J. Lewis, M. Meinshausen, Z. Nicholls, P. Patel, S. Ragnauth, J. Rogelj, S. Waldhoff, S. Yu and H. McJeon, *Science*, 2021, **374**, 693–695.
13 J. Rogelj, O. Fricko, M. Meinshausen, V. Krey, J. J. J. Zilliacus and K. Riahi, *Nat. Commun.*, 2017, **8**, 1–12.
14 N. A. of S. and N. A. of E. Institute of Medicine, *Policy Implications of Greenhouse Warming: Mitigation, Adaptation, and the Science Base*, National Academies Press, Washington, DC, 1992.
15 T. M. Lenton and N. E. Vaughan, *Atmos. Chem. Phys.*, 2009, **9**, 5539–5561.
16 J. von Neumann, *Fortune*, 1955, 106–108.
17 D. L. Mitchell and W. Finnegan, *Environ. Res. Lett.*, 2009, **4**, 045102.
18 P. J. Crutzen, *Clim. Change*, 2006, **77**, 211–220.
19 T. Chen, W. B. Rossow and Y. Zhang, *J. Clim.*, 2000, **13**, 264–286.
20 T. Storelvmo and N. Herger, *J. Geophys. Res.*, 2014, **119**, 2375–2389.
21 T. Storelvmo, W. R. Boos and N. Herger, *Philos. Trans. R. Soc., A*, 2014, **372**(2031), DOI: **10.1098/rsta.2014.0116**.
22 J. E. Kristjánsson, H. Muri and H. Schmidt, *Geophys. Res. Lett.*, 2015, **42**, 10807–10815.
23 T. Storelvmo, J. E. Kristjansson, H. Muri, M. Pfeffer, D. Barahona and A. Nenes, *Geophys. Res. Lett.*, 2013, **40**, 178–182.
24 J. E. Penner, C. Zhou and X. Liu, *Geophys. Res. Lett.*, 2015, **42**, 8775–8782.
25 B. Gasparini and U. Lohmann, *J. Geophys. Res.: Atmos.*, 2016, **121**, 4877–4893.
26 C. Tully, D. Neubauer, N. Omanovic and U. Lohmann, *Atmos. Chem. Phys.*, 2022, **22**, 11455–11484.
27 B. Gasparini, Z. McGraw, T. Storelvmo and U. Lohmann, *Environ. Res. Lett.*, 2020, **15**, 054002.
28 P. J. Irvine, A. Ridgwell and D. J. Lunt, *J. Geophys. Res.: Atmos.*, 2011, **116**, 24112.
29 A. Ridgwell, J. S. Singarayer, A. M. Hetherington and P. J. Valdes, *Curr. Biol.*, 2009, **19**, 146–150.
30 R. M. Hamwey, *Mitig. Adapt. Strateg. Glob. Change*, 2007, **12**, 419–439.
31 A. Rosenfeld, J. Romm, H. Akbari and A. Lloyd, *MIT Technol. Rev.*, 1997, 100(2), pp. 52–59.
32 H. Akbari, S. Menon and A. Rosenfeld, *Clim. Change*, 2008, **94**, 275–286.
33 J. Mandal, Y. Yang, N. Yu and A. P. Raman, *Joule*, 2020, **4**, 1350–1356.
34 T. R. Loveland, B. C. Reed, J. F. Brown, D. O. Ohlen, Z. Zhu, L. Yang and J. W. Merchant, *Int. J. Remote Sens.*, 2000, **21**, 1303–1330.
35 H. Taha, *Energy Build.*, 1997, **25**, 99–103.
36 A. Trlica, L. R. Hutyra, C. L. Schaaf, A. Erb and J. A. Wang, *Earth's Future*, 2017, **5**, 1084–1101.
37 M. Z. Jacobson and J. E. Ten Hoeve, *J. Clim.*, 2012, **25**, 1028–1044.
38 K. W. Oleson, G. B. Bonan and J. Feddema, *Geophys. Res. Lett.*, 2010, **37**, 3701.
39 *Heat Island Cooling Strategies | Heat Island Effect | US EPA*, **https://www.epa.gov/heatislands/heat-island-cooling-strategies**, (accessed 12 July 2021).
40 J. Latham, *Nature*, 1990, **347**, 339–340.
41 J. Latham, *Atmos. Sci. Lett.*, 2002, **3**, 52–58.
42 S. Twomey, *J. Atmos. Sci.*, 1977, **34**, 1149–1152.
43 B. A. Albrecht, *Science*, 1989, **245**, 1227–1230.
44 J. Latham, P. Rasch, C.-C. Chen, L. Kettles, A. Gadian, A. Gettelman, H. Morrison, K. Bower and T. Choularton, *Philos. Trans. R. Soc., A*, 2008, **366**, 3969–3987.
45 K. J. Noone, E. Öström, R. J. Ferek, T. Garrett, P. V. Hobbs, D. W. Johnson, J. P. Taylor, L. M. Russell, R. C. Flagan, J. H. Seinfeld, C. D. O'Dowd, M. H. Smith, P. A. Durkee, K. Nielsen, J. G. Hudson, R. A. Pockalny, L. De Bock, R. E. Van Grieken, R. F. Gasparovic and I. Brooks, *J. Atmos. Sci.*, 2000, **57**, 2729–2747.
46 D. A. Randall, J. A. Coakley Jr., C. W. Fairall, R. A. Kropfli and D. H. Lenschow, *Bull. Am. Meteorol. Soc.*, 1984, **65**, 1290–1301.

47 P. J. Rasch, J. Latham and C.-C. (J.) Chen, *Environ. Res. Lett.*, 2009, **4**, 045112.
48 Y. C. Chen, M. W. Christensen, L. Xue, A. Sorooshian, G. L. Stephens, R. M. Rasmussen and J. H. Seinfeld, *Atmos. Chem. Phys.*, 2012, **12**, 8223–8235.
49 A.-I. Partanen, H. Kokkola, S. Romakkaniemi, V.-M. Kerminen, K. E. J. Lehtinen, T. Bergman, A. Arola and H. Korhonen, *J. Geophys. Res.: Atmos.*, 2012, **117**, 2203.
50 A. Jones, J. Haywood and O. Boucher, *J. Geophys. Res.: Atmos.*, 2009, **114**, 10106.
51 H. M. Horowitz, C. Holmes, A. Wright, T. Sherwen, X. Wang, M. Evans, J. Huang, L. Jaeglé, Q. Chen, S. Zhai and B. Alexander, *Geophys. Res. Lett.*, 2020, **47**, e2019GL085838.
52 G. Cooper, D. Johnston, J. Foster, L. Galbraith, A. Neukermans, R. Ormond, J. Rush, Q. Wang, G. Cooper, D. Johnston, J. Foster, L. Galbraith, A. Neukermans, R. Ormond, J. Rush and Q. Wang, *Int. J. Geosci.*, 2013, **4**, 78–97.
53 A. K. L. Jenkins, P. M. Forster and L. S. Jackson, *Atmos. Chem. Phys.*, 2013, **13**, 1659–1673.
54 A. K. L. Jenkins and P. M. Forster, *Atmos. Sci. Lett.*, 2013, **14**, 164–169.
55 H. Muri, U. Niemeier and J. E. Kristjánsson, *Geophys. Res. Lett.*, 2015, **42**, 2951–2960.
56 K. Bower, T. Choularton, J. Latham, J. Sahraei and S. Salter, *Atmos. Res.*, 2006, **82**, 328–336.
57 H. Korhonen, K. S. Carslaw and S. Romakkaniemi, *Atmos. Chem. Phys.*, 2010, **10**, 4133–4143.
58 L. Ahlm, A. Jones, W. C. Stjern, H. Muri, B. Kravitz and J. E. Kristjánsson, *Atmos. Chem. Phys.*, 2017, **17**, 13071–13087.
59 C. W. Stjern, H. Muri, L. Ahlm, O. Boucher, J. N. S. Cole, D. Ji, A. Jones, J. Haywood, B. Kravitz, A. Lenton, J. C. Moore, U. Niemeier, S. J. Phipps, H. Schmidt, S. Watanabe and J. E. Kristjánsson, *Atmos. Chem. Phys.*, 2018, **18**, 621–634.
60 R. Wood, *Atmos. Chem. Phys.*, 2021, **21**, 14507–14533.
61 P. J. Irvine, B. Kravitz, M. G. Lawrence and H. Muri, *Wiley Interdiscip. Rev. Clim. Change*, 2016, **7**, 815–833.
62 M. K. Mcnutt, W. Abdalati, K. Caldeira, S. C. Doney, P. G. Falkowski, S. Fetter, J. R. Fleming, S. P. Hamburg, M. G. Morgan and J. E. Penner, *Climate Intervention: Reflecting Sunlight to Cool Earth*, The National Academies Press, Washington, D.C., 2015.
63 P. J. Irvine, B. Kravitz, M. G. Lawrence, D. Gerten, C. Caminade, S. N. Gosling, E. J. Hendy, B. T. Kassie, W. D. Kissling, H. Muri, A. Oschlies and S. J. Smith, *Earth's Future*, 2017, **5**, 93–106.
64 M. G. Lawrence, S. Schäfer, H. Muri, V. Scott, A. Oschlies, N. E. Vaughan, O. Boucher, H. Schmidt, J. Haywood and J. Scheffran, *Nat. Commun.*, 2018, **9**, 1–19.
65 M. I. Budyko, *Tellus*, 1977, **29**, 193–204.
66 K. Labitzke and M. P. McCormick, *Geophys. Res. Lett.*, 1992, **19**, 207–210.
67 W. B. Grant, J. Fishman, E. V. Browell, V. G. Brackett, D. Nganga, A. Minga, B. Cros, R. E. Veiga, C. F. Butler, M. A. Fenn and G. D. Nowicki, *Geophys. Res. Lett.*, 1992, **19**, 1109–1112.
68 M. P. McCormick, L. W. Thomason and C. R. Trepte, *Nature*, 1995, **373**, 399–404.
69 M. J. Mills, J. H. Richter, S. Tilmes, B. Kravitz, D. G. Macmartin, A. A. Glanville, J. J. Tribbia, J. F. Lamarque, F. Vitt, A. Schmidt, A. Gettelman, C. Hannay, J. T. Bacmeister and D. E. Kinnison, *J. Geophys. Res.: Atmos.*, 2017, **122**, 13061–13078.
70 S. Driscoll, A. Bozzo, L. J. Gray, A. Robock and G. Stenchikov, *J. Geophys. Res.: Atmos.*, 2012, **117**, 17105.
71 R. B. Stothers, *Science*, 1984, **224**, 1191–1198.
72 L. L. Stowe, R. M. Carey and P. P. Pellegrino, *Geophys. Res. Lett.*, 1992, **19**, 159–162.
73 C. S. Long and L. L. Stowe, *Geophys. Res. Lett.*, 1994, **21**, 2215–2218.
74 G. K. Yue, M. P. McCormick and E. W. Chiou, *J. Geophys. Res.: Atmos.*, 1991, **96**, 5209–5219.
75 M. P. McCormick and R. E. Veiga, *Geophys. Res. Lett.*, 1992, **19**, 155–158.
76 K. Labitzke, B. Naujokat and M. P. McCormick, *Geophys. Res. Lett.*, 1983, **10**, 24–26.
77 D. E. Parker and J. L. Brownscombe, *Nature*, 1983, **301**, 406–408.
78 E. G. Dutton and J. R. Christy, *Geophys. Res. Lett.*, 1992, **19**, 2313–2316.
79 D. J. Hofmann and S. Solomon, *J. Geophys. Res.*, 1989, **94**, 5029.
80 F. J. Dentener and P. J. Crutzen, *J. Geophys. Res.: Atmos.*, 1993, **98**, 7149–7163.
81 P. Heckendorn, D. Weisenstein, S. Fueglistaler, B. P. Luo, E. Rozanov, M. Schraner, L. W. Thomason and T. Peter, *Environ. Res. Lett.*, 2009, **4**, 045108.
82 A. E. Dessler, M. R. Schoeberl, T. Wang, S. M. Davis and K. H. Rosenlof, *Proc. Natl. Acad. Sci. U. S. A.*, 2013, **110**, 18087–18091.
83 M. M. Joshi, A. J. Charlton and A. A. Scaife, *Geophys. Res. Lett.*, 2006, **33**, L09806.
84 A. C. Maycock, M. M. Joshi, K. P. Shine and A. A. Scaife, *J. Clim.*, 2013, **26**, 545–561.
85 A. J. Ferraro, E. J. Highwood and A. J. Charlton-Perez, *Environ. Res. Lett.*, 2014, **9**, 014001.
86 B. Kravitz, A. Robock, D. T. Shindell and M. A. Miller, *J. Geophys. Res.: Atmos.*, 2012, **117**(D9), D09203.
87 A. C. Jones, J. M. Haywood and A. Jones, *Atmos. Chem. Phys.*, 2016, **16**, 2843–2862.
88 Q. Tang, P. G. Hess, B. Brown-Steiner and D. E. Kinnison, *Geophys. Res. Lett.*, 2013, **40**, 5553–5558.
89 L. Xia, P. J. Nowack, S. Tilmes and A. Robock, *Atmos. Chem. Phys.*, 2017, **17**, 11913–11928.
90 S. Kinne, O. B. Toon and M. J. Prather, *Geophys. Res. Lett.*, 1992, **19**, 1927–1930.
91 G. Pitari and E. Mancini, *Nat. Hazards Earth Syst. Sci.*, 2002, **2**, 91–108.
92 V. Aquila, L. D. Oman, R. S. Stolarski, P. R. Colarco and P. A. Newman, *J. Geophys. Res.: Atmos.*, 2012, **117**, 6216.

93 V. Aquila, L. D. Oman, R. Stolarski, A. R. Douglass and P. A. Newman, *J. Atmos. Sci.*, 2013, **70**, 894–900.
94 L. Millán, M. L. Santee, A. Lambert, N. J. Livesey, F. Werner, M. J. Schwartz, H. C. Pumphrey, G. L. Manney, Y. Wang, H. Su, L. Wu, W. G. Read and L. Froidevaux, *Geophys. Res. Lett.*, 2022, **49**, e2022GL099381.
95 H. Vömel, S. Evan and M. Tully, *Science*, 2022, **377**, 1444–1447.
96 Y. Zhu, C. G. Bardeen, S. Tilmes, M. J. Mills, X. Wang, V. L. Harvey, G. Taha, D. Kinnison, R. W. Portmann, P. Yu, K. H. Rosenlof, M. Avery, C. Kloss, C. Li, A. S. Glanville, L. Millán, T. Deshler, N. Krotkov and O. B. Toon, *Commun. Earth Environ.*, 2022, **3**, 1–7.
97 P. Sellitto, A. Podglajen, R. Belhadji, M. Boichu, E. Carboni, J. Cuesta, C. Duchamp, C. Kloss, R. Siddans, N. Bègue, L. Blarel, F. Jegou, S. Khaykin, J. B. Renard and B. Legras, *Commun. Earth Environ.*, 2022, **3**, 1–10.
98 A. F. Bais, C. S. Zerefos, I. C. Ziomas, N. Zoumakis, H. T. Mantis, D. J. Hofmann and G. Fiocco, *Atmos. Ozone*, 1985, 353–356.
99 H. T. Mantis, C. S. Zerefos, A. Baise, I. Ziomas and A. Kelessis, *Arch. Meteorol., Geophys. Bioclimatol., Ser. B*, 1986, **36**, 135–145.
100 J. F. Gleason, P. K. Bhartia, J. R. Herman, R. McPeters, P. Newman, R. S. Stolarski, L. Flynn, G. Labow, D. Larko, C. Seftor, C. Wellemeyer, W. D. Komhyr, A. J. Miller and W. Planet, *Science*, 1993, **260**, 523–526.
101 J. R. Herman and D. Larko, *J. Geophys. Res.: Atmos.*, 1994, **99**, 3483–3496.
102 G. Pitari, V. Aquila, B. Kravitz, A. Robock, S. Watanabe, I. Cionni, N. Luca, G. Genova, E. Mancini and S. Tilmes, *J. Geophys. Res.*, 2014, **119**, 2629–2653.
103 *Ultraviolet Radiation in Antarctica: Measurements and Biological Effects*, ed. C. S. Weiler and P. A. Penhale, American Geophysical Union, Washington, D. C., 1994, vol. 62.
104 J. C. van der Leun, X. Tang and M. Tevini, *Environmental Effects of Ozone Depletion: 1998 Assessment*, 1998.
105 D. G. MacMartin, B. Kravitz, J. C. S. Long and P. J. Rasch, *Earth's Future*, 2016, **4**, 543–548.
106 B. Kravitz and D. G. MacMartin, *Nat. Rev. Earth Environ.*, 2020, **1**, 64–75.
107 S. Tilmes, D. Visioni, A. Jones, J. Haywood, R. Séférian, P. Nabat, O. Boucher, E. M. Bednarz and U. Niemeier, *Atmos. Chem. Phys.*, 2022, **22**, 4557–4579.
108 A. Robock, D. G. MacMartin, R. Duren and M. W. Christensen, *Clim. Change*, 2013, **121**, 445–458.
109 D. G. Macmartin, B. Kravitz, S. Tilmes, J. H. Richter, M. J. Mills, J. F. Lamarque, J. J. Tribbia and F. Vitt, *J. Geophys. Res.: Atmos.*, 2017, **122**, 12574–12590.
110 WMO, *Scientific Assessment of Ozone Depletion, GAW Report No. 278*, Geneva, Switzerland, 2022, p. 56.
111 S. D. Eastham, D. K. Weisenstein, D. W. Keith and S. R. H. Barrett, *Atmos. Environ.*, 2018, **187**, 424–434.
112 S. Madronich, S. Tilmes, B. Kravitz, D. G. MacMartin and J. H. Richter, *Atmos*, 2018, **9**, 432.
113 D. W. Keith, *Annu. Rev. Energy Environ.*, 2003, **25**, 245–284.
114 J. Reynolds, *Anthr. Rev.*, 2014, **2**(2), 174–191.
115 D. McLaren, *Earth's Future*, 2016, **4**, 596–602.
116 M. M. K. Austin and B. A. Converse, *J. Environ. Psychol.*, 2021, **78**, 101690.
117 D. A. Dana, *AESS Interdiscip. Environ. Stud. Sci. Ser.*, 2021, 165–181.
118 T. M. Andrews, A. W. Delton and R. Kline, *Ecol. Econ.*, 2022, **196**, 107421.
119 T. L. Cherry, S. Kroll, D. M. McEvoy, D. Campoverde and J. Moreno-Cruz, *Environ. Polit.*, 2022, **32**(2), 362–370.
120 H. D. Matthews and K. Caldeira, *Proc. Natl. Acad. Sci. U. S. A.*, 2007, **104**, 9949–9954.
121 J. F. Tjiputra, A. Grini and H. Lee, *J. Geophys. Res.: Biogeosci.*, 2016, **121**, 2–27.
122 D. W. Keith, G. Wagner and C. L. Zabel, *Nat. Clim. Change*, 2017, **7**, 617–619.
123 K. S. Lauvset, J. Tjiputra and H. Muri, *Biogeosciences*, 2017, **14**, 5675–5691.
124 J. T. Fasullo, S. Tilmes, J. H. Richter, B. Kravitz, D. G. MacMartin, M. J. Mills and I. R. Simpson, *Nat. Geosci.*, 2018, **11**, 910–914.
125 D. P. Keller, E. Y. Feng and A. Oschlies, *Nat. Commun.*, 2014, **5**, 1–11.
126 M. Plazzotta, R. Séférian and H. Douville, *Earth's Future*, 2019, **7**, 664–676.
127 A. Parker and P. J. Irvine, *Earth's Future*, 2018, **6**, 456–467.
128 B. J. Soden, R. T. Wetherald, G. L. Stenchikov and A. Robock, *Science*, 2002, **296**, 727–730.
129 J. Haywood and O. Boucher, *Rev. Geophys.*, 2000, **38**, 513–543.
130 S. Kremser, L. W. Thomason, M. von Hobe, M. Hermann, T. Deshler, C. Timmreck, M. Toohey, A. Stenke, J. P. Schwarz, R. Weigel, S. Fueglistaler, F. J. Prata, J. P. Vernier, H. Schlager, J. E. Barnes, J. C. Antuña-Marrero, D. Fairlie, M. Palm, E. Mahieu, J. Notholt, M. Rex, C. Bingen, F. Vanhellemont, A. Bourassa, J. M. C. Plane, D. Klocke, S. A. Carn, L. Clarisse, T. Trickl, R. Neely, A. D. James, L. Rieger, J. C. Wilson and B. Meland, *Rev. Geophys.*, 2016, **54**, 278–335.
131 J. X. Sheng, D. K. Weisenstein, B. P. Luo, E. Rozanov, A. Stenke, J. Anet, H. Bingemer and T. Peter, *J. Geophys. Res.*, 2015, **120**, 256–276.
132 P. J. Crutzen, *Geophys. Res. Lett.*, 1976, **3**, 73–76.
133 W. R. Stockwell and J. G. Calvert, *Atmos. Environ.*, 1983, **17**, 2231–2235.
134 F. Lehner, A. P. Schurer, G. C. Hegerl, C. Deser and T. L. Frölicher, *Geophys. Res. Lett.*, 2016, **43**, 2851–2858.
135 S. Tilmes, J. H. Richter, M. J. Mills, B. Kravitz, D. G. MacMartin, R. R. Garcia, D. E. Kinnison, J. F. Lamarque, J. Tribbia and F. Vitt, *J. Geophys. Res.: Atmos.*, 2018, **123**, 4654–4673.
136 S. Tilmes, J. H. Richter, M. J. Mills, B. Kravitz, D. G. Macmartin, F. Vitt, J. J. Tribbia and J. F. Lamarque, *J. Geophys. Res.: Atmos.*, 2017, **122**, 12591–12615.
137 D. Visioni, D. G. MacMartin, B. Kravitz, S. Tilmes, M. J. Mills, J. H. Richter and M. P. Boudreau, *Geophys. Res. Lett.*, 2019, **46**, 7790–7799.

138 C. A. Brock, H. H. Jonsson, J. C. Wilson, J. E. Dye, D. Baumgardner, S. Borrmann, M. C. Pitts, M. T. Osborn, R. J. DeCoursey and D. C. Woods, *Geophys. Res. Lett.*, 1993, **20**, 2555–2558.
139 D. M. Murphy, K. D. Froyd, I. Bourgeois, C. A. Brock, A. Kupc, J. Peischl, G. P. Schill, C. R. Thompson, C. J. Williamson and P. Yu, *Atmos. Chem. Phys.*, 2021, **21**, 8915–8932.
140 A. J. Ferraro, E. J. Highwood and A. J. Charlton-Perez, *Geophys. Res. Lett.*, 2011, **38**, 24706.
141 F. D. Pope, P. Braesicke, R. G. Grainger, M. Kalberer, I. M. Watson, P. J. Davidson and R. A. Cox, *Nat. Clim. Change*, 2012, **2**, 713–719.
142 D. K. Weisenstein, D. W. Keith and J. A. Dykema, *Atmos. Chem. Phys.*, 2015, **15**, 11835–11859.
143 D. W. Keith, D. K. Weisenstein, J. A. Dykema and F. N. Keutsch, *Proc. Natl. Acad. Sci. U. S. A.*, 2016, **113**, 14910–14914.
144 A. Lacis, J. Hansen and M. Sato, *Geophys. Res. Lett.*, 1992, **19**, 1607–1610.
145 F. P. J. Valero and P. Pilewskie, *Geophys. Res. Lett.*, 1992, **19**, 163–166.
146 P. B. Russell, J. M. Livingston, E. G. Dutton, R. F. Pueschel, J. A. Reagan, T. E. DeFoor, M. A. Box, D. Allen, P. Pilewskie, B. M. Herman, S. A. Kinne and D. J. Hofmann, *J. Geophys. Res.: Atmos.*, 1993, **98**, 22969–22985.
147 P. J. Rasch, S. Tilmes, R. P. Turco, A. Robock, L. Oman, C.-C. (J.) Chen, G. L. Stenchikov and R. R. Garcia, *Philos. Trans. R. Soc., A*, 2008, **366**, 4007–4037.
148 F. Benduhn and M. G. Lawrence, *J. Geophys. Res.: Atmos.*, 2013, **118**, 7905–7921.
149 U. Lohmann and J. Feichter, *Atmos. Chem. Phys.*, 2005, **5**, 715–737.
150 U. Lohmann, *Geophys. Res. Lett.*, 2002, **29**, 11.
151 P. J. DeMott, A. J. Prenni, X. Liu, S. M. Kreidenweis, M. D. Petters, C. H. Twohy, M. S. Richardson, T. Eidhammer and D. C. Rogers, *Proc. Natl. Acad. Sci. U. S. A.*, 2010, **107**, 11217–11222.
152 P. J. Rasch, P. J. Crutzen and D. B. Coleman, *Geophys. Res. Lett.*, 2008, **35**(2), DOI: **10.1029/2007GL032179**.
153 K. E. Trenberth and A. Dai, *Geophys. Res. Lett.*, 2007, **34**(15), DOI: **10.1029/2007GL030524**.
154 A. Robock, L. Oman and G. L. Stenchikov, *J. Geophys. Res.: Atmos.*, 2008, **113**, 16101.
155 A. Jones, J. Haywood, O. Boucher, B. Kravitz and A. Robock, *Atmos. Chem. Phys.*, 2010, **10**, 5999–6006.
156 S. Tilmes, J. Fasullo, J. F. Lamarque, D. R. Marsh, M. Mills, K. Alterskjær, H. Muri, J. E. Kristjánsson, O. Boucher, M. Schulz, J. N. S. Cole, C. L. Curry, A. Jones, J. Haywood, P. J. Irvine, D. Ji, J. C. Moore, D. B. Karam, B. Kravitz, P. J. Rasch, B. Singh, J. H. Yoon, U. Niemeier, H. Schmidt, A. Robock, S. Yang and S. Watanabe, *J. Geophys. Res.: Atmos.*, 2013, **118**, 11036–11058.
157 K. Sassen, *Science*, 1992, **257**, 516–519.
158 A. Schmidt, K. S. Carslaw, G. W. Mann, A. Rap, K. J. Pringle, D. V. Spracklen, M. Wilson and P. M. Forster, *Atmos. Chem. Phys.*, 2012, **12**, 7321–7339.
159 P. Forster, V. Ramaswamy, P. Artaxo, T. Berntsen, R. Betts, D. W. Fahey, J. Haywood, J. Lean, D. C. Lowe, G. Myhre, J. Nganga, R. Prinn, G. Raga, M. Schulz and R. Van Dorland, in *Climate Change 2007: The Physical Science Basis. Contribution of Working Group I to the Fourth Assessment Report of the Intergovernmental Panel on Climate Change*, ed. S. Solomon, D. Qin, M. Manning, Z. Chen, M. Marquis, K. B. Averyt, M. Tignor and H. L. Miller, Cambridge University Press, Cambridge, United Kingdom and New York, NY, USA, 2007.
160 A. Laor and B. T. Draine, *Astrophys. J.*, 1993, **402**, 441.
161 J. A. Dykema, D. W. Keith and F. N. Keutsch, *Geophys. Res. Lett.*, 2016, **43**, 7758–7766.
162 C. E. Jung, C. W. Chagnon and J. E. Manson, *J. Meteorol.*, 1961, **18**, 81–108.
163 X. Tie, G. P. Brasseur, B. Briegleb and C. Granier, *J. Geophys. Res.*, 1994, **99**, 20545.
164 M. Kuebbeler, U. Lohmann and J. Feichter, *Geophys. Res. Lett.*, 2012, **39**, 23803.
165 G. L. Stenchikov, I. Kirchner, A. Robock, H.-F. Graf, J. C. Antuña, R. G. Grainger, A. Lambert and L. Thomason, *J. Geophys. Res.: Atmos.*, 1998, **103**, 13837–13857.
166 N. G. Andronova, E. V. Rozanov, F. Yang, M. E. Schlesinger and G. L. Stenchikov, *J. Geophys. Res.: Atmos.*, 1999, **104**, 16807–16826.
167 S. Ramachandran, V. Ramaswamy, G. L. Stenchikov and A. Robock, *J. Geophys. Res.: Atmos.*, 2000, **105**, 24409–24429.
168 U. Niemeier, H. Schmidt and C. Timmreck, *Atmos. Sci. Lett.*, 2011, **12**, 189–194.
169 C. R. Trepte, R. E. Veiga and M. P. McCormick, *J. Geophys. Res.: Atmos.*, 1993, **98**, 18563–18573.
170 M. H. Hitchman, M. McKay and C. R. Trepte, *J. Geophys. Res.: Atmos.*, 1994, **99**, 20689–20700.
171 M. A. Thomas, M. A. Giorgetta, C. Timmreck, H. F. Graf and G. Stenchikov, *Atmos. Chem. Phys.*, 2009, **9**, 3001–3009.
172 J. P. Pinto, R. P. Turco and O. B. Toon, *J. Geophys. Res.: Atmos.*, 1989, **94**, 11165–11174.
173 M. Sato, J. E. Hansen, M. P. McCormick and J. B. Pollack, *J. Geophys. Res.: Atmos.*, 1993, **98**, 22987–22994.
174 Y. Fujii, *J. Atmos. Sol.–Terr. Phys.*, 2011, **73**, 643–652.
175 S. Tilmes, R. R. Garcia, D. E. Kinnison, A. Gettelman and P. J. Rasch, *J. Geophys. Res.: Atmos.*, 2009, **114**(D12), DOI: **10.1029/2008JD011420**.
176 A. C. Jones, J. M. Haywood, N. Dunstone, K. Emanuel, M. K. Hawcroft, K. I. Hodges and A. Jones, *Nat. Commun.*, 2017, **8**, 1–10.
177 J. Proctor, S. Hsiang, J. Burney, M. Burke and W. Schlenker, *Nature*, 2018, **560**, 480–483.
178 Z. Dai, D. K. Weisenstein, F. N. Keutsch and D. W. Keith, *Commun. Earth Environ.*, 2020, **1**, 1–9.
179 D. Visioni, D. G. Macmartin, B. Kravitz, O. Boucher, A. Jones, T. Lurton, M. Martine, M. J. Mills, P. Nabat, U. Niemeier, R. Séférian and S. Tilmes, *Atmos. Chem. Phys.*, 2021, **21**, 10039–10063.
180 M. Meinshausen, S. J. Smith, K. Calvin, J. S. Daniel, M. L. T. Kainuma, J.-F. Lamarque, K. Matsumoto,

S. A. Montzka, S. C. B. Raper, K. Riahi, A. Thomson, G. J. M. Velders and D. P. P. van Vuuren, *Clim. Change*, 2011, **109**, 213–241.
181 S. Tilmes, M. J. Mills, U. Niemeier, H. Schmidt, A. Robock, B. Kravitz, J. F. Lamarque, G. Pitari and J. M. English, *Geosci. Model Dev.*, 2015, **8**, 43–49.
182 B. Kravitz, A. Robock, O. Boucher, H. Schmidt, K. E. Taylor, G. Stenchikov and M. Schulz, *Atmos. Sci. Lett.*, 2011, **12**, 162–167.
183 W. Smith, *Environ. Res. Lett.*, 2020, **15**, 114004.
184 H. N. Huynh and V. F. McNeill, *J. Phys. Chem. A*, 2020, **124**, 3886–3895.
185 T. C. Bond, S. J. Doherty, D. W. Fahey, P. M. Forster, T. Berntsen, B. J. Deangelo, M. G. Flanner, S. Ghan, B. Kärcher, D. Koch, S. Kinne, Y. Kondo, P. K. Quinn, M. C. Sarofim, M. G. Schultz, M. Schulz, C. Venkataraman, H. Zhang, S. Zhang, N. Bellouin, S. K. Guttikunda, P. K. Hopke, M. Z. Jacobson, J. W. Kaiser, Z. Klimont, U. Lohmann, J. P. Schwarz, D. Shindell, T. Storelvmo, S. G. Warren and C. S. Zender, *J. Geophys. Res.: Atmos.*, 2013, **118**, 5380–5552.
186 B. Kravitz, D. G. MacMartin and K. Caldeira, *Geophys. Res. Lett.*, 2012, **39**, 11801.
187 L. M. Mercado, N. Bellouin, S. Sitch, O. Boucher, C. Huntingford, M. Wild and P. M. Cox, *Nat*, 2009, **458**, 1014–1017.
188 S. Solomon, R. R. Garcia, F. S. Rowland and D. J. Wuebbles, *Nature*, 1986, **321**, 755–758.
189 M. J. Molina, T. L. Tso, L. T. Molina and F. C. Y. Wang, *Science*, 1987, **238**, 1253–1257.
190 J. P. D. Abbatt and M. J. Molina, *J. Phys. Chem.*, 1992, **96**, 7674–7679.
191 J. P. D. Abbatt and M. J. Molina, *Geophys. Res. Lett.*, 1992, **19**, 461–464.
192 D. R. Hanson and A. R. Ravishankara, *J. Phys. Chem.*, 1992, **96**, 2682–2691.
193 D. W. Fahey, S. R. Kawa, E. L. Woodbridge, P. Tin, J. C. Wilson, H. H. Jonsson, J. E. Dye, D. Baumgardner, S. Borrmann, D. W. Toohey, L. M. Avallone, M. H. Proffitt, J. Margitan, M. Loewenstein, J. R. Podolske, R. J. Salawitch, S. C. Wofsy, M. K. W. Ko, D. E. Anderson, M. R. Schoeber and K. R. Chan, *Nature*, 1993, **363**, 509–514.
194 D. W. Fahey, E. R. Keim, K. A. Boering, C. A. Brock, J. C. Wilson, H. H. Jonsson, S. Anthony, T. F. Hanisco, P. O. Wennberg, R. C. Miake-Lye, R. J. Salawitch, N. Louisnard, E. L. Woodbridge, R. S. Gao, S. G. Donnelly, R. C. Wamsley, L. A. Del Negro, S. Solomon, B. C. Daube, S. C. Wofsy, C. R. Webster, R. D. May, K. K. Kelly, M. Loewenstein, J. R. Podolske and K. R. Chan, *Science*, 1995, **270**, 70–74.
195 G. Taubes, *Science*, 1993, **260**, 1580–1583.
196 S. E. Strahan and A. R. Douglass, *Geophys. Res. Lett.*, 2018, **45**, 382–390.
197 L. M. Western, M. K. Vollmer, P. B. Krummel, K. E. Adcock, P. J. Fraser, C. M. Harth, R. L. Langenfelds, S. A. Montzka, J. Mühle, S. O'Doherty, D. E. Oram, S. Reimann, M. Rigby, I. Vimont, R. F. Weiss, D. Young and J. C. Laube, *Nat. Geosci.*, 2023, **16**, 309–313.
198 R. L. Thompson, L. Lassaletta, P. K. Patra, C. Wilson, K. C. Wells, A. Gressent, E. N. Koffi, M. P. Chipperfield, W. Winiwarter, E. A. Davidson, H. Tian and J. G. Canadell, *Nat. Clim. Change*, 2019, **9**, 993–998.
199 H. Tian, R. Xu, J. G. Canadell, R. L. Thompson, W. Winiwarter, P. Suntharalingam, E. A. Davidson, P. Ciais, R. B. Jackson, G. Janssens-Maenhout, M. J. Prather, P. Regnier, N. Pan, S. Pan, G. P. Peters, H. Shi, F. N. Tubiello, S. Zaehle, F. Zhou, A. Arneth, G. Battaglia, S. Berthet, L. Bopp, A. F. Bouwman, E. T. Buitenhuis, J. Chang, M. P. Chipperfield, S. R. S. Dangal, E. Dlugokencky, J. W. Elkins, B. D. Eyre, B. Fu, B. Hall, A. Ito, F. Joos, P. B. Krummel, A. Landolfi, G. G. Laruelle, R. Lauerwald, W. Li, S. Lienert, T. Maavara, M. MacLeod, D. B. Millet, S. Olin, P. K. Patra, R. G. Prinn, P. A. Raymond, D. J. Ruiz, G. R. van der Werf, N. Vuichard, J. Wang, R. F. Weiss, K. C. Wells, C. Wilson, J. Yang and Y. Yao, *Nat*, 2020, **586**, 248–256.
200 W. G. Mankin, M. T. Coffey and A. Goldman, *Geophys. Res. Lett.*, 1992, **19**, 179–182.
201 L. Wallace and W. Livingston, *Geophys. Res. Lett.*, 1992, **19**, 1209.
202 A. Tabazadeh and R. P. Turco, *Science*, 1993, **260**, 1082–1086.
203 S. Kutterolf, T. H. Hansteen, A. Freundt, H. Wehrmann, K. Appel, K. Krüger and W. Pérez, *Earth Planet. Sci. Lett.*, 2015, **429**, 234–246.
204 C. M. Vidal, N. Métrich, J. C. Komorowski, I. Pratomo, A. Michel, N. Kartadinata, V. Robert and F. Lavigne, *Sci. Rep.*, 2016, **6**, 1–13.
205 J. Eric Klobas, D. M. Wilmouth, D. K. Weisenstein, J. G. Anderson and R. J. Salawitch, *Geophys. Res. Lett.*, 2017, **44**, 7490–7499.
206 H. Brenna, S. Kutterolf and K. Krüger, *Sci. Rep.*, 2019, **9**, 1–14.
207 G. A. Millard, T. A. Mather, D. M. Pyle, W. I. Rose and B. Thornton, *Geophys. Res. Lett.*, 2006, **33**, 19815.
208 W. I. Rose, G. A. Millard, T. A. Mather, D. E. Hunton, B. Anderson, C. Oppenheimer, B. F. Thornton, T. M. Gerlach, A. A. Viggiano, Y. Kondo, T. M. Miller and J. O. Ballenthin, *J. Geophys. Res.: Atmos.*, 2006, **111**, 20206.
209 G. P. Brasseur, C. Granier and S. Walters, *Nature*, 1990, **348**, 626–628.
210 J. M. Rodriguez, M. K. W. Ko and N. D. Sze, *Nature*, 1991, **352**, 134–137.
211 S. Solomon, G. H. Mount, R. W. Sanders, R. O. Jakoubek and A. L. Schmeltekopf, *Science*, 1988, **242**, 550–555.
212 M. Prather, *J. Geophys. Res.: Atmos.*, 1992, **97**, 10187–10191.
213 G. Brasseur and C. Granier, *Science*, 1992, **257**, 1239–1242.
214 D. J. Hofmann, S. J. Oltmans, J. M. Harris, W. D. Komhyr, J. A. Lathrop, T. DeFoor and D. Kuniyuki, *Geophys. Res. Lett.*, 1993, **20**, 1555–1558.
215 M. R. Schoeberl, P. K. Bhartia, E. Hilsenrath and O. Torres, *Geophys. Res. Lett.*, 1993, **20**, 29–32.

216 D. J. Hofmann, S. J. Oltmans, W. D. Komhyr, J. M. Harris, J. A. Lathrop, A. O. Langford, T. Deshler, B. J. Johnson, A. Torres and W. A. Matthews, *Geophys. Res. Lett.*, 1994, **21**, 65–68.
217 T. Deshler, A. Adriani, G. P. Gobbi, D. J. Hofmann, G. Di Donfrancesco and B. J. Johnson, *Geophys. Res. Lett.*, 1992, **19**, 1819–1822.
218 R. G. Grainger, A. Lambert, C. D. Rodgers, F. W. Taylor and T. Deshler, *J. Geophys. Res.: Atmos.*, 1995, **100**, 16507–16518.
219 M. J. Mills, A. O. Langford, T. J. O'Leary, K. Arpag, H. L. Miller, M. H. Proffitt, R. W. Sanders and S. Solomon, *Geophys. Res. Lett.*, 1993, **20**, 1187–1190.
220 P. V. Johnston, R. L. McKenzie, J. G. Keys and W. A. Matthews, *Geophys. Res. Lett.*, 1992, **19**, 211–213.
221 M. Koike, Y. Kondo, W. A. Matthews, P. V. Johnston and K. Yamazaki, *Geophys. Res. Lett.*, 1993, **20**, 1975–1978.
222 P. V. Johnston and R. L. McKenzie, *J. Geophys. Res.: Atmos.*, 1989, **94**, 3473–3486.
223 C. R. Webster, R. D. May, M. Allen, L. Jaeglé and M. P. McCormick, *Geophys. Res. Lett.*, 1994, **21**, 53–56.
224 M. Koike, N. B. Jones, W. A. Matthews, P. V. Johnston, R. L. McKenzie, D. Kinnison and J. Rodriguez, *Geophys. Res. Lett.*, 1994, **21**, 597–600.
225 C. S. Zerefos, K. Tourpali and A. F. Bais, *J. Geophys. Res.: Atmos.*, 1994, **99**, 25741–25746.
226 W. J. Randel, F. Wu, J. M. Russell, J. W. Waters and L. Froidevaux, *J. Geophys. Res.: Atmos.*, 1995, **100**, 16753–16764.
227 W. J. Randel and F. Wu, *J. Atmos. Sci.*, 1996, **53**, 2546–2559.
228 M. J. Prather, M. M. García, A. R. Douglass, C. H. Jackman, M. K. W. Ko and N. D. Sze, *J. Geophys. Res.: Atmos.*, 1990, **95**, 18583–18590.
229 T. Hinklin, B. Toury, C. Gervais, F. Babonneau, J. J. Gislason, R. W. Morton and R. M. Laine, *Chem. Mater.*, 2003, **16**, 21–30.
230 T. Tsuzuki and P. G. McCormick, *J. Mater. Sci.*, 2004, **39**, 5143–5146.
231 M. N. Ross and P. M. Sheaffer, *Earth's Future*, 2014, **2**, 177–196.
232 C. H. Jackman, D. B. Considine and E. L. Fleming, *J. Geophys. Res.: Atmos.*, 1996, **101**, 12523–12529.
233 C. H. Jackman, D. B. Considine and E. L. Fleming, *Geophys. Res. Lett.*, 1998, **25**, 907–910.
234 M. Y. Danilin, R.-L. Shia, M. K. W. Ko, D. K. Weisenstein, N. D. Sze, J. J. Lamb, T. W. Smith, P. D. Lohn and M. J. Prather, *J. Geophys. Res.: Atmos.*, 2001, **106**, 12727–12738.
235 M. J. Molina, L. T. Molina, R. Zhang, R. F. Meads and D. D. Spencer, *Geophys. Res. Lett.*, 1997, **24**, 1619–1622.
236 F. Hanisch and J. N. Crowley, *Atmos. Chem. Phys.*, 2003, **3**, 119–130.
237 C. R. Usher, A. E. Michel and V. H. Grassian, *Chem. Rev.*, 2003, **103**, 4883–4939.
238 T. Ibusuki and K. Takeuchi, *J. Mol. Catal.*, 1994, **88**, 93–102.
239 Y. Ohko, Y. Nakamura, A. Fukuda, S. Matsuzawa and K. Takeuchi, *J. Phys. Chem. C*, 2008, **112**, 10502–10508.
240 M. Ndour, B. D'Anna, C. George, O. Ka, Y. Balkanski, J. Kleffmann, K. Stemmler and M. Ammann, *Geophys. Res. Lett.*, 2008, **35**(5), DOI: **10.1029/2007GL032006**.
241 Y. Bedjanian and A. El Zein, *J. Phys. Chem. A*, 2012, **116**, 1758–1764.
242 D. P. Dee, S. M. Uppala, A. J. Simmons, P. Berrisford, P. Poli, S. Kobayashi, U. Andrae, M. A. Balmaseda, G. Balsamo, P. Bauer, P. Bechtold, A. C. M. Beljaars, L. van de Berg, J. Bidlot, N. Bormann, C. Delsol, R. Dragani, M. Fuentes, A. J. Geer, L. Haimberger, S. B. Healy, H. Hersbach, E. V. Hólm, L. Isaksen, P. Kållberg, M. Köhler, M. Matricardi, A. P. McNally, B. M. Monge-Sanz, J.-J. Morcrette, B.-K. Park, C. Peubey, P. de Rosnay, C. Tavolato, J.-N. Thépaut and F. Vitart, *Q. J. R. Meteorol. Soc.*, 2011, **137**, 553–597.
243 D. R. Hanson, A. R. Ravishankara and S. Solomon, *J. Geophys. Res.: Atmos.*, 1994, **99**, 3615–3629.
244 F. F. Fenter, F. Caloz and M. J. Rossi, *Atmos. Environ.*, 1995, **29**, 3365–3372.
245 G. M. Underwood, P. Li, C. R. Usher and V. H. Grassian, *J. Phys. Chem. A*, 2000, **104**, 819–829.
246 A. L. Goodman, G. M. Underwood and V. H. Grassian, *J. Geophys. Res.: Atmos.*, 2000, **105**, 29053–29064.
247 F. Hanisch and J. N. Crowley, *J. Phys. Chem. A*, 2001, **105**, 3096–3106.
248 E. R. Johnson, J. Sciegienka, S. Carlos-Cuellar and V. H. Grassian, *J. Phys. Chem. A*, 2005, **109**, 6901–6911.
249 A. Vlasenko, S. Sjogren, E. Weingartner, K. Stemmler, H. W. Gäggeler and M. Ammann, *Atmos. Chem. Phys.*, 2006, **6**, 2147–2160.
250 C. Santschi and M. J. Rossi, *J. Phys. Chem. A*, 2006, **110**, 6789–6802.
251 F. Karagulian, C. Santschi and M. J. Rossi, *Atmos. Chem. Phys.*, 2006, **6**, 1373–1388.
252 P. K. Mogili, P. D. Kleiber, M. A. Young and V. H. Grassian, *Atmos. Environ.*, 2006, **40**, 7401–7408.
253 C. Wagner, F. Hanisch, N. Holmes, H. de Coninck, G. Schuster and J. N. Crowley, *Atmos. Chem. Phys.*, 2008, **8**, 91–109.
254 C. Wagner, G. Schuster and J. N. Crowley, *Atmos. Environ.*, 2009, **43**, 5001–5008.
255 G. M. Underwood, C. H. Song, M. Phadnis, G. R. Carmichael and V. H. Grassian, *J. Geophys. Res.: Atmos.*, 2001, **106**, 18055–18066.
256 G. M. Underwood, P. Li, H. Al-Abadleh and V. H. Grassian, *J. Phys. Chem. A*, 2001, **105**, 6609–6620.
257 A. L. Goodman, E. T. Bernard and V. H. Grassian, *J. Phys. Chem. A*, 2001, **105**, 6443–6457.
258 S. Seisel, C. Börensen, R. Vogt and R. Zellner, *Phys. Chem. Chem. Phys.*, 2004, **6**, 5498–5508.
259 M. J. Tang, P. J. Telford, F. D. Pope, L. Rkiouak, N. L. Abraham, A. T. Archibald, P. Braesicke, J. A. Pyle, J. McGregor, I. M. Watson, R. A. Cox and M. Kalberer, *Atmos. Chem. Phys.*, 2014, **14**, 6035–6048.
260 M. Tang, J. Keeble, P. J. Telford, F. D. Pope, P. Braesicke, P. T. Griffiths, N. Luke Abraham, J. McGregor, I. Matt

Watson, R. Anthony Cox, J. A. Pyle and M. Kalberer, *Atmos. Chem. Phys.*, 2016, **16**, 15397–15412.
261 D. R. Moon, G. S. Taverna, C. Anduix-Canto, T. Ingham, M. P. Chipperfield, P. W. Seakins, M. T. Baeza-Romero and D. E. Heard, *Atmos. Chem. Phys.*, 2018, **18**, 327–338.
262 Y. Liu, E. R. Gibson, J. P. Cain, H. Wang, A. V. H. Grassian and A. Laskin, *J. Phys. Chem. A*, 2008, **112**, 1561–1571.
263 H. N. Huynh and V. F. McNeill, *ACS Earth Space Chem.*, 2021, **5**, 1896–1901.
264 C. R. Usher, A. E. Michel, D. Stec and V. H. Grassian, *Atmos. Environ.*, 2003, **37**, 5337–5347.
265 S. Tilmes, R. Müller and R. Salawitch, *Science*, 2008, **320**, 1201–1204.
266 B. C. O'Neill, C. Tebaldi, D. P. Van Vuuren, V. Eyring, P. Friedlingstein, G. Hurtt, R. Knutti, E. Kriegler, J. F. Lamarque, J. Lowe, G. A. Meehl, R. Moss, K. Riahi and B. M. Sanderson, *Geosci. Model Dev.*, 2016, **9**, 3461–3482.
267 S. Tilmes, D. E. Kinnison, R. R. Garcia, R. Salawitch, T. Canty, J. Lee-Taylor, S. Madronich and K. Chance, *Atmos. Chem. Phys.*, 2012, **12**, 10945–10955.
268 P. J. Nowack, N. L. Abraham, P. Braesicke and J. A. Pyle, *Atmos. Chem. Phys.*, 2016, **16**, 4191–4203.
269 S. J. Oltmans, A. S. Lefohn, H. E. Scheel, J. M. Harris, H. Levy, I. E. Galbally, E. G. Brunke, C. P. Meyer, J. A. Lathrop, B. J. Johnson, D. S. Shadwick, E. Cuevas, F. J. Schmidlin, D. W. Tarasick, H. Claude, J. B. Kerr, O. Uchino and V. Mohnen, *Geophys. Res. Lett.*, 1998, **25**, 139–142.
270 A. C. Fusco and J. A. Logan, *J. Geophys. Res.: Atmos.*, 2003, **108**, 4449.
271 K. E. Trenberth, *Clim. Change*, 1999, **42**, 327–339.
272 K. E. Trenberth, A. Dai, R. M. Rasmussen and D. B. Parsons, *Bull. Am. Meteorol. Soc.*, 2003, **84**, 1205–1218.
273 I. M. Held and B. J. Soden, *J. Clim.*, 2006, **19**, 5686–5699.
274 G. Bala, P. B. Duffy and K. E. Taylor, *Proc. Natl. Acad. Sci. U. S. A.*, 2008, **105**, 7664–7669.
275 J. M. Haywood, A. Jones, N. Bellouin and D. Stephenson, *Nat. Clim. Change*, 2013, **3**, 660–665.
276 I. R. Simpson, S. Tilmes, J. H. Richter, B. Kravitz, D. G. MacMartin, M. J. Mills, J. T. Fasullo and A. G. Pendergrass, *J. Geophys. Res.: Atmos.*, 2019, **124**, 12587–12616.
277 C. E. Iles and G. C. Hegerl, *Nat. Geosci.*, 2015, **8**, 838–842.
278 D. G. MacMartin, W. Wang, B. Kravitz, S. Tilmes, J. H. Richter and M. J. Mills, *J. Geophys. Res.: Atmos.*, 2019, **124**, 1233–1247.
279 J. C. Moore, A. Grinsted, X. Guo, X. Yu, S. Jevrejeva, A. Rinke, X. Cui, B. Kravitz, A. Lenton, S. Watanabe and D. Ji, *Proc. Natl. Acad. Sci. U. S. A.*, 2015, **112**, 13794–13799.
280 P. Irvine, K. Emanuel, J. He, L. W. Horowitz, G. Vecchi and D. Keith, *Nat. Clim. Change*, 2019, **9**, 295–299.
281 F. S. R. Pausata and S. J. Camargo, *Proc. Natl. Acad. Sci. U. S. A.*, 2019, **116**, 7732–7737.
282 A. T. Evan, *J. Geophys. Res.: Atmos.*, 2012, **117**, D06101.
283 A. Guevara-Murua, E. J. Hendy, A. C. Rust and K. V. Cashman, *Geophys. Res. Lett.*, 2015, **42**, 9425–9432.
284 M. Latif, N. Keenlyside and J. Bader, *Geophys. Res. Lett.*, 2007, **34**(1), L01710.
285 G. Villarini and G. A. Vecchi, *J. Clim.*, 2013, **26**, 3231–3240.
286 N. J. Dunstone, D. M. Smith, B. B. B. Booth, L. Hermanson and R. Eade, *Nat. Geosci.*, 2013, **6**, 534–539.
287 K. A. Emanuel, *Proc. Natl. Acad. Sci. U. S. A.*, 2013, **110**, 12219–12224.
288 S. J. Camargo, *J. Clim.*, 2013, **26**, 9880–9902.
289 K. J. E. Walsh, S. J. Camargo, G. A. Vecchi, A. S. Daloz, J. Elsner, K. Emanuel, M. Horn, Y.-K. Lim, M. Roberts, C. Patricola, E. Scoccimarro, A. H. Sobel, S. Strazzo, G. Villarini, M. Wehner, M. Zhao, J. P. Kossin, T. LaRow, K. Oouchi, S. Schubert, H. Wang, J. Bacmeister, P. Chang, F. Chauvin, C. Jablonowski, A. Kumar, H. Murakami, T. Ose, K. A. Reed, R. Saravanan, Y. Yamada, C. M. Zarzycki, P. L. Vidale, J. A. Jonas and N. Henderson, *Bull. Am. Meteorol. Soc.*, 2015, **96**, 997–1017.
290 B. E. Brown, *Coral Reefs*, 1997, **16**, S129–S138.
291 O. Hoegh-Guldberg, *Mar. Freshwater Res.*, 1999, **50**, 839–866.
292 A. J. Edwards, S. Clark, H. Zahir, A. Rajasuriya, A. Naseer and J. Rubens, *Mar. Pollut. Bull.*, 2001, **42**, 7–15.
293 C. Langdon and M. J. Atkinson, *J. Geophys. Res.: Oceans*, 2005, **110**, 1–16.
294 N. C. S. Chan and S. R. Connolly, *Global Change Biol.*, 2013, **19**, 282–290.
295 C. A. Schloss, T. A. Nuñez and J. J. Lawler, *Proc. Natl. Acad. Sci. U. S. A.*, 2012, **109**, 8606–8611.
296 R. T. Corlett and D. A. Westcott, *Trends Ecol. Evol.*, 2013, **28**, 482–488.
297 C. H. Trisos, G. Amatulli, J. Gurevitch, A. Robock, L. Xia and B. Zambri, *Nat. Ecol. Evol.*, 2018, **2**, 475–482.
298 S. R. Loarie, P. B. Duffy, H. Hamilton, G. P. Asner, C. B. Field and D. D. Ackerly, *Nature*, 2009, **462**, 1052–1055.
299 I.-C. Chen, J. K. Hill, R. Ohlemüller, D. B. Roy and C. D. Thomas, *Science*, 2011, **333**, 1024–1026.
300 M. T. Burrows, D. S. Schoeman, L. B. Buckley, P. Moore, E. S. Poloczanska, K. M. Brander, C. Brown, J. F. Bruno, C. M. Duarte, B. S. Halpern, J. Holding, C. V. Kappel, W. Kiessling, M. I. O'Connor, J. M. Pandolfi, C. Parmesan, F. B. Schwing, W. J. Sydeman and A. J. Richardson, *Science*, 2011, **334**, 652–655.
301 M. L. Pinsky, B. Worm, M. J. Fogarty, J. L. Sarmiento and S. A. Levin, *Science*, 2013, **341**, 1239–1242.
302 M. T. Burrows, D. S. Schoeman, A. J. Richardson, J. G. Molinos, A. Hoffmann, L. B. Buckley, P. J. Moore, C. J. Brown, J. F. Bruno, C. M. Duarte, B. S. Halpern, O. Hoegh-Guldberg, C. V. Kappel, W. Kiessling, M. I. O'Connor, J. M. Pandolfi, C. Parmesan, W. J. Sydeman, S. Ferrier, K. J. Williams and E. S. Poloczanska, *Nat*, 2014, **507**, 492–495.
303 B. Sandel, L. Arge, B. Dalsgaard, R. G. Davies, K. J. Gaston, W. J. Sutherland and J.-C. Svenning, *Science*, 2011, **334**, 660–664.
304 UN Environment Programme, *Conference of the Parties to the Convention on Biological Diversity, Tenth meeting*, Nagoya, Japan, 2010, pp. 82–353.

305 National Academies of Sciences, Engineering, and Medicine, *Reflecting Sunlight: Recommendations for Solar Geoengineering Research and Research Governance*, The National Academies Press, Washington, DC, 2021.
306 H. J. Buck, A. R. Gammon and C. J. Preston, *Hypatia*, 2014, **29**, 651–669.
307 D. E. Winickoff, J. A. Flegal and A. Asrat, *Nat. Clim. Change*, 2015, **5**, 627–634.
308 S. Jinnah, S. Nicholson and J. Flegal, *Ethics Policy Environ.*, 2018, **21**, 362–381.
309 J. A. Flegal, A. M. Hubert, D. R. Morrow and J. B. Moreno-Cruz, *Annu. Rev. Environ. Resour.*, 2019, **44**, 399–423.
310 D. G. MacMartin, P. J. Irvine, B. Kravitz and J. B. Horton, *Clim. Policy*, 2019, **19**, 1325–1339.
311 B. Kravitz, D. G. MacMartin, D. T. Leedal, P. J. Rasch and A. J. Jarvis, *Environ. Res. Lett.*, 2014, **9**, 044006.
312 D. G. MacMartin, B. Kravitz and P. J. Rasch, *Geophys. Res. Lett.*, 2015, **42**, 7156–7161.
313 B. Kravitz, D. G. Macmartin, H. Wang and P. J. Rasch, *Earth Syst. Dyn.*, 2016, **7**, 469–497.
314 B. Kravitz, D. G. MacMartin, M. J. Mills, J. H. Richter, S. Tilmes, J.-F. Lamarque, J. J. Tribbia and F. Vitt, *J. Geophys. Res.: Atmos.*, 2017, **122**, 12616–12634.
315 *Putting Developing Countries at the Centre of the SRM Conversation*, **https://www.degrees.ngo/**, (accessed 3 August 2023).
316 A. E. Alamou, E. Obada, E. I. Biao, E. B. J. Zandagba, C. Y. Da-Allada, F. K. Bonou, E. Baloïtcha, S. Tilmes, P. Irvine, A. Sharifi, C. Feng, J. Yang, A. E. Alamou, E. Obada, E. I. Biao, E. Babadjidé, J. Zandagba, C. Y. Da-Allada, F. K. Bonou, E. Baloïtcha, S. Tilmes and P. J. Irvine, *Atmos*, 2022, **13**, 234.
317 M. L. Tan, L. Juneng, H. Kuswanto, H. X. Do and F. Zhang, *Water*, 2023, **15**, 1089.
318 I. Pinto, C. Jack, C. Lennard, S. Tilmes and R. C. Odoulami, *Geophys. Res. Lett.*, 2020, **47**, e2019GL086047.
319 C. J. Carlson, R. Colwell, M. S. Hossain, M. M. Rahman, A. Robock, S. J. Ryan, M. S. Alam and C. H. Trisos, *Nat. Commun.*, 2022, **13**, 1–9.
320 S. Schäfer, P. J. Irvine, A. M. Hubert, D. Reichwein, S. Low, H. Stelzer, A. Maas and M. G. Lawrence, *Nat. Clim. Change*, 2013, **3**, 766.
321 J. L. Reynolds, *Clim. Law*, 2015, 182–209.
322 A. A. Rahman, P. Artaxo, A. Asrat and A. Parker, *Nature*, 2018, **556**, 22–24.
323 R. Rayfuse, in *The Oxford Handbook of Law, Regulation and Technology*, 2017, pp. 799–822.
324 J. L. Reynolds, *Proc. R. Soc. A*, 2019, **475**(2229), DOI: **10.1098/rspa.2019.0255**.
325 P. MacNaghten and R. Owen, *Nature*, 2011, **479**, 293.
326 *Why A Landmark Experiment Into Dimming the Sun Got Canceled | Grist*, **https://grist.org/science/who-gets-to-decide-if-we-study-solar-geoengineering-after-the-scopex-project-canceled/**, (accessed 28 June 2021).
327 *Open Letter to SCoPEx Advisory Committee – Geoengineering Monitor*, **https://www.geoengineeringmonitor.org/2019/08/open-letter-scopex/**, (accessed 28 June 2021).
328 J. McClellan, D. W. Keith and J. Apt, *Environ. Res. Lett.*, 2012, **7**, 034019.
329 R. Moriyama, M. Sugiyama, A. Kurosawa, K. Masuda, K. Tsuzuki and Y. Ishimoto, *Mitig. Adapt. Strateg. Glob. Change*, 2016, **22**, 1207–1228.
330 W. Smith and G. Wagner, *Environ. Res. Lett.*, 2018, **13**, 124001.
331 U. Niemeier and C. Timmreck, *Atmos. Chem. Phys.*, 2015, **15**, 9129–9141.
332 K. Dagon and D. P. Schrag, *Clim. Change*, 2019, **153**, 235–251.
333 C. L. Curry, J. Sillmann, D. Bronaugh, K. Alterskjaer, J. N. S. Cole, D. Ji, B. Kravitz, J. E. Kristjánsson, J. C. Moore, H. Muri, U. Niemeier, A. Robock, S. Tilmes and S. Yang, *J. Geophys. Res.: Atmos.*, 2014, **119**, 3900–3923.
334 A. Jones, J. M. Haywood, K. Alterskjær, O. Boucher, J. N. S. Cole, C. L. Curry, P. J. Irvine, D. Ji, B. Kravitz, J. Egill Kristjánsson, J. C. Moore, U. Niemeier, A. Robock, H. Schmidt, B. Singh, S. Tilmes, S. Watanabe and J.-H. Yoon, *J. Geophys. Res.: Atmos.*, 2013, **118**, 9743–9752.
335 K. E. McCusker, K. C. Armour, C. M. Bitz and D. S. Battisti, *Environ. Res. Lett.*, 2014, **9**, 024005.
336 U. Effiong and R. L. Neitzel, *Environ. Health*, 2016, **15**, 7.
337 R. Baan, K. Straif, Y. Grosse, B. Secretan, F. El Ghissassi and V. Cogliano, *Lancet Oncol.*, 2006, **7**, 295–296.
338 B. Kravitz, A. Robock, L. Oman, G. Stenchikov and A. B. Marquardt, *J. Geophys. Res.: Atmos.*, 2009, **114**, 14109.
339 K. Caldeira, G. Bala and L. Cao, *Annu. Rev. Earth Planet. Sci.*, 2013, **41**, 231–256.
340 D. Visioni, G. Pitari, G. Di Genova, S. Tilmes and I. Cionni, *Atmos. Chem. Phys.*, 2018, **18**, 14867–14887.